THE LAMPF STATUS AND DEVELOPMENT

Louis Rosen

Los Alamos Scientific Laboratory

Los Alamos, New Mexico

I. INTRODUCTION: DEFINITION OF LAMPF

Eight years ago, at Yerevan, I gave a talk at the VII International Conference on High Energy Accelerators. In that talk I described a linear proton accelerator which was to provide the basis for a meson factory facility. The accelerator was to be in three stages and provide variable energy up to 800 MeV. The design intensity was to be 1000 μA and the duty factor 6%. The duty factor, and intensity and energy were all formidable extrapolations for linacs, from what was then available.

The meson factory, which I described eight years ago at a meeting in the Soviet Union, has now been successfully completed.

At the moment LAMPF is the largest and most diversified nuclear science facility in the world. It gives promise to remain so for the foreseeable future even though it will have strong competition from meson factories in Canada, Switzerland and one under construction in the USSR.

The LAMPF is based on a proton accelerator of variable energy up to 800 MeV, and of design intensity 1 mA scheduled for 1980. We are presently operating at 150 μA average current.

The major thrust of LAMPF is to bridge the gap between nuclear and subnuclear physics by addressing families of problems crucial to each and common to both, to explore practical applications of accelerator beams and accelerator technologies and to provide an arena for inter-discipline research and education.

II. SCIENTIFIC MOTIVATION OF LAMPF

Figure 1 shows LAMPF goals as originally identified more than a decade ago. They have changed very little since. Several hundred scientists from approximately 75 U.S. and foreign institutions are attacking the indicated problems. They encompass the entire spectrum from atomic physics to neutrino physics, and from such basic and esoteric questions as the rare decay modes of the muon to the treatment of cancer with negative pions.

III. LAMPF PHYSICAL PLANT

On March 20, 1969, LAMPF looked as shown in Fig. 2. Today it looks as shown in Fig. 2a. It is a linear accelerator pointing directly at Washington, D.C.

Figure 3 shows schematically the injector complex. Three injectors are utilized. Two beams, one H^+ and the other H^-, are accelerated simultaneously. A polarized H^- beam was achieved last week. A photograph of one of the three injectors is shown in Fig. 4. Figure 5 shows the second stage of the accelerator - the Alvarez or drift-tube section. Figure 6 shows the main stage, developed at LASL by Nagle and Knapp and their collaborators, and representing a dramatic advance in accelerator technology. The rf systems designed by Hagerman, Jameson, Boyd and their colleagues are no less novel, especially the rf control circuitry and the comprehensive computer control system, which development was led by Harold Butler.

No less challenging than the accelerator has been the switchyard, main beam lines and secondary beam lines, including target systems and beam stop. This effort was led by Lewis Agnew, Robert Macek and their colleagues.

Figure 7 shows the switchyard and experimental areas. An important feature of LAMPF, emphasized by the energy crisis, is the capability to provide beam to as many as 13 experiments simultaneously.

Figure 8 illustrates the complexity of a target cell, which must be serviced remotely. This requirement provides, however, an opportunity to develop sophisticated master-slave, force-reflective, servomanipulator systems which can be of great importance to a nuclear reactor economy. Figure 8a shows a remote manipulator system. Figure 9 shows one of the channels - the stopped muon channel and Fig. 10 shows the high resolution proton spectrometer. Figure 10a indicates the kind of results obtainable with that instrument.

An indication of the quality of LAMPF beam is given by Fig. 11. Primary beam can occupy a phase space of 0.1 mr mm.

A. Multiple Coulomb Scattering (Fig. 11).

IV. BASIC RESEARCH PROGRAM

A. Atomic Physics

1. Resonances in the Photo-Disassociation of H^-. UNM and LASL

It is fashionable these days to exploit colliding beam experiments. We can't afford to build colliding beams so we do it with mirrors. Figure 12 shows how.

This is an atomic physics experiment which I included because I thought it might intrigue Professor Rabi. The purpose is to detect and understand, in terms of classical quantum mechanics, the resonances encountered in the photo-disassociation of H^-.

Figure 13 shows some initial results.

The shape resonance is unperturbed by magnetic fields that were applied. But the Feshbach resonance exhibits marvelous versatility. It splits first into two and then into three resonances and exhibits broadening as the magnetic field is increased.

2. Spectroscopy of muonium. Yale, LASL, Heidelberg, Bern

Figure 14 shows the energy level diagrams for muonium in its ground state and Fig. 15 the results of a monumental effort, conducted by the Yale group under Professor Vernon Hughes, to measure with exquisite precision the hyperfine splitting structure interval ($\Delta\nu$) for muonium. The hfs was measured to a precision of 0.1 ppm leading to a value of the magnetic moment of the muon, relative to the proton, to an accuracy of better than 1 ppm. All of this bears, of course, very directly on quantum electrodynamics. The hyperfine splitting (HFS) interval ($\Delta\nu$) in the ground state of muonium was measured to very high precision in both a weak and strong field experiment.

Weak Field (<2 mG): $(F,M_f) = (1,\pm 1) \rightarrow 0.0$.

Strong Field (13.6 kG): $(M_J,M) = (1/2,1/2)\ (1/2,-1/2)$

and

$(-1/2,-1/2)\ (-1/2,1/2)$.

Some formidable technological hurdles had to be surmounted. A high precision eighth order solenoid, designed and constructed at Yale, provided a magnetic field stable to 1 ppm and homogeneous to 4 ppm over a region 19-cm long and 19 cm in diameter in which resided the microwave cavity. The microwave system provides ∿50 W of 1.9 GH_z to 2.5 GH_z power stabilized in frequency to 0.01 ppm.

B. Nuclear Chemistry (Separate but equal facilities.)

Perhaps for the first time in the U.S.A., a large accelerator complex included in its design and construction essentially everything the nuclear chemists wanted. We have provided them separate but equal facilities. Our faith in our nuclear chemistry colleagues has been more than justified.

1. Observation of New Nuclides at LAMPF. LBL, LASL

Nuclides ^{27}Ne, ^{31}Mg, ^{32}Mg, ^{34}Al and ^{39}P have been observed as a result of the bombardment of uranium by 800 MeV protons in the thin target area of the switchyard.

The technique indicated in Fig. 16 involves the use of the rf microstructure to provide time-of-flight measurements, along with ΔE and total E determinations. The intensity of LAMPF permits very long flight paths and hence good resolution. Since many micropulses are involved, a short flight path is also used to identify the relevant rf pulse against which timing is done. In this experiment, in the neutrino experiments and in others, the pulsed nature of linacs is used to good advantage. Figure 17 shows mass spectra for the elements Ne, Mg, Al and P, indicating newly discovered isotopes. The mass surface is, of course, one of the fundamental characteristics of nuclear matter. It appears that this technique is accurate enough to do mass spectroscopy over a substantial portion of the periodic table, and for very short-lived nuclei.

2. Polyneutron Systems.

Searches for polyneutron systems have thus far been unsuccessful.

3. Isotope Production at LAMPF.

Figure 18 shows the Radioisotope Production Facility. We recently produced fourteen curies of ^{88}Y. LAMPF is the only accelerator in the world which could produce sufficient quantity in a time comparable to the 100-day half-life.

The ^{82}Sr-^{82}Rb generator has been produced. The ^{82}Rb is used in heart infarction studies and blood flow studies. A process for producing pure ^{123}I is under development.

C. Nuclear Physics

1. Total Pi-Nucleus Cross Sections. U. of Montana, U. of Washington, LASL, New Mexico State

Nuclear charge distributions can now be well determined from electron scattering and muonic x-ray data. Nuclear matter distributions, and particularly neutron (rms) radii are not known with comparable precision. Reasonably accurate determinations of (rms) neutron radii and very accurate determinations of differences between neutron radii in isotopes can be made through pion total cross sections because of the isospin coupling of the π-nucleon system through the (3-3) resonance.

The main problems are corrections for coulomb-nuclear interference which essentially cancel if radii differences of isotopes are being compared. In that case models also predict nearly the same cross section differences even though different models may predict widely different cross sections for a given isotope. It is this model independence which permits the determination of relative neutron radii. In cases where we believe $r_p = r_n$ as for doubly closed shell nuclei such as ^{40}Ca and ^{16}O, accurate absolute neutron (rms) radii can be determined for the various isotopes. Electron scattering data show that r_p (^{48}Ca) = r_p (^{40}Ca) and r_p (^{18}O) = r_p (^{16}O). Predictions for differences between total cross sections for isotopes can be obtained from the optical model.

Some qualitative features of the curves in Fig. 19 may be understood from free π-nucleon scattering. The σ_t is approximately equal to the free π^--neutron cross section times the number of unshielded neutrons outside the absorbing core of ^{16}O. The point where all the curves cross is where the model predicts the core nucleus to be essentially transparent. Ninety mb is approximately twice the π^- neutron cross section at this energy. The cross-over point is model independent.

Above 150 MeV there is little model dependence. Below 150 MeV there is substantial model dependence. At higher energies one can therefore extract model-independent structural information which can perhaps be then used to extract details of dynamics at lower energies.

Problems:

1) Coulomb scattering
2) Coulomb-nuclear interference
3) Finite size of target
4) Pion decay in flight
5) Interactions in the beam detectors.

2. E_2 Nuclear Resonance Effect in Pionic Atoms.

Subject effect occurs when the energy difference between atomic levels is nearly equal to the energy of an excited state of the nucleus, Fig. 20. Configuration mixing is then produced by the coulomb field and this is manifested as attenuation of the pionic x-ray line compared to that of an isotope. This effect has been observed in Cd, Pa, and Ru.

The results confirm an interesting prediction made by Ericson some years ago that the zero energy p-wave π-nucleus potential becomes repulsive as Z increases beyond $\sim$36. The nuclear p-wave interaction includes contributions from the π-nucleon s-waves (repulsive) and π-nucleon p-waves (attractive). At some point the s-wave contribution overtakes the p-wave one and the resultant potential should change sign. This it appears to do. One uses a phenomenological potential to calculate the pionic level shifts and widths. In Pd (z = 46) the π-nucleus potential has become repulsive.

3. $\pi^+ + d \rightarrow p + p$. U. of South Carolina, LASL, ORNL, VPI

Objective: Obtain information about the deuteron d-state probability. The fast protons emitted carry information about the high momentum components of the deuteron, particularly the percent d-state. Figure 21 shows the experimental arrangement. Figure 22 illustrates some results. BCM refers to the Lomon-Feshbach boundary condition model wave functions with 7.6% and 4.6% d-state probabilities.

4. $\pi^- + T \rightarrow 3n + \pi$. LBL

Purpose: Search for the existence of a 3-neutron bound state of T = 3/2 resonance in the 3-body system. Most work on this problem is confused by the existence of a fourth strongly interacting particle. Crowe avoided this by observing the photon (in a pair spectrometer) produced after π^- captures on tritium. Preliminary results are shown in Fig. 23. Approximately 20,000 curies of T were used.

5. Double Charge Exchange. LASL, U. of South Carolina, ANL

Figure 24 shows the results of a rather exotic experiment performed by Burman, et al. The ^{18}Ne ground state is a double isobaric analogue of the ^{18}O ground state. No other ^{18}Ne states are populated below the particle emission threshold. It appears that pion double charge exchange may be useful as a spectroscopic tool.

The experimental method, Fig. 25, is unique. The LEP channel was set up with the first two dipoles acting as a spectrometer for the incident π^+ beam and the last two acting as a spectrometer for the emitted π^-. The target was at midpoint. Data were taken at 0^o.

6. Muonic Atom Physics.

Here the basic physics we think we understand. The information which muonic atoms yield is very precise because there is almost no shielding from the electronic cloud and we essentially have a "one electron" atom. Because of the μ-mass, the μ orbit reflects the effect of the finite size of the nuclear charge distribution for both ground and also nuclear states excited by the mixing of atomic and nuclear wave functions.

A particularly neat experiment was performed by the Cal Tech group on ^{165}Ho. They measured muonic transition energies as well as the hyperfine splitting for the 3d and 2p levels, thereby obtaining information not only about the radial moments but also about the E2 and E4 static moments of the ground state. Figure 26 shows contour plots of the angular distribution (r,θ) for a cut through the poles and normalized to 100% charge density at the center. The solid curves are for constant skin thickness while in the dashed ones the skin thickness was allowed to vary. The shape used to extract these numbers was a Fermi charge distribution with parameters C and t which depend on θ, the azimuthal angle:

$$\rho(r) = \rho_0 \left[1 + \exp 4.4 \frac{(r-c)}{t}\right]$$

7. P-Nucleus Interactions at Large Scattering Angles. U. of PA, LASL

Although most experiments at LAMPF have been done with pions and muons, some are done with protons and neutrons. The HRS system consists of a beam line optically matched to QDD spectrometer in such a way, that for a two-body nuclear process the outgoing particles reveal the population of final residual nuclear states independent of the incident or scattered particle momenta. Figure 27 indicates the resolution of the system.

A particularly interesting experiment on back scattering of protons from nuclei has been done by Frankel and associates. Analysis is based on a concept of Amado and Woloshyn according to which the back scattering cross section resulting from protons on nuclei should be dominated by the lowest internal momentum of a nucleon which can produce the observed external momentum of the backward emerging particle. This concept reflects the fact that the internal momentum distribution falls very rapidly as a function of mementum. Figure 28 shows some of the experimental results. Model is that a proton collides with a nucleon.

Sherman Frankel concludes that the experimental data are consistent with the hypothesis that the interactions which produce backward particles can be represented by single scattering from a high momentum distribution

$$F(K) = \frac{e^{-} k/k_0}{K}$$

where K is the momentum of the virtual nucleon.

D. Particle Physics

1. Direct Positron Production in p-p Collisions.

a. Motivation

(1) Theoretical Advice. An eminent theorist once advised me that there are only two circumastances which warrant an experiment. One occurs when theorists say that they need some data to proceed with or test their models. The second occurs when theorists believe they know the results an experiment will yield. In the present case, both criteria were met.

(2) Previous data at high energies give one direct lepton for 10^4 pions, almost independent of incident energy. This is higher than can be accounted for by existing models.

(3) Is there a threshold for direct positron production?

(4) Are they due to a low mass object?

(5) Is there a continuity of $e^+ e^-$ masses?

b. Experimental Arrangement

(1) Figure 29 illustrates experimental arrangement.

(a) Single-arm spectrometer with good electron identification and reasonable momentum resolution.

(b) Positrons produced in collision of proton beam with a liquid hydrogen target.

(c) Main b.g. was from pair production from γ's and π^o-Dalitz decay. These were determined by adding absorbers between target and first counter and then extrapolating to zero.

c. Results

(1) Figure 30 illustrates the results.

2. Rare Decay Modes of Pions and Muons.

a. Introduction

It would appear that the best things in life are illegal, immoral, fattening or have a low probability of occurring, which brings us to rare decay modes.

b. Pion Decay Modes to be Investigated at LAMPF

(1) Figure 31 indicates some of the pion decay modes to be addressed at LAMPF.

(a) Preliminary data have been obtained on the pion beta-decay. The full scale experiment will be mounted when LAMPF achieves 300 μA at beam. The motivation for this experiment is that a really precise result could confront, in a definitive way, predictions of the Conserved Vector Current (CVC) form of the weak interaction. The decay rate is proportional to the product of the weak coupling constant and the Cabibbo angle.

(b) $\pi \rightarrow e\gamma$ tests μ-e universality.

(c) $\pi^o \rightarrow \gamma\gamma\gamma$ tests C conservation. This experiment should get on the floor next year on the LEP channel.

(d) The π^0 Dalitz decay rate has been run on P^3. The data look good but analysis is not yet complete. A 1% measurement is hoped for. Figure 32 shows a schematic of the experimental arrangement, and Fig. 33 a photograph. The π^- beam is incident on a CH_2 target. The e^+e^- pair are detected with a magnetic spectrometer and the associated gamma in a shower counter. The Dalitz ratio is determined by taking data with various thicknesses of Cu converter in front of the spectrometer and extrapolating to zero thickness.

(e) $\pi^0 \rightarrow e^+e^-$. The same experimental arrangement is being used to detect the $\pi^0 \rightarrow e^+e^-$ decay which has a unitarily lower bound relative to $\pi^0 \rightarrow \gamma\gamma$ of 4.7×10^{-8}. Assuming a given Feynman diagram, this ratio can be calculated using QED, which you saw from the experiments of Professor Hughes' group is quite reliable.

3. Lepton Conservation

The discovery of two types of neutrinos led most physicists to believe that muon and lepton numbers are separately conserved. However, recent developments in gauge theories suggest that this need not be so. Two experiments are under way at LAMPF to investigate lepton number violation. Figure 34 illustrates and experiment to test lepton conservation and neutrino oscillations.

a. $\mu^+ \to e^+ + \nu_e + \bar{\nu}_\mu$

or

b. $\mu^+ \to e^+ + \bar{\nu}_e + \nu_\mu$

c. $\bar{\nu}_\mu \to \bar{\nu}_e$?

Electron neutrinos (or anti-neutrinos) enter an H_2O (or D_2O) Cerenkov counter protected from charged particles by an anti-coincidence scintillator array. Neutron b.g. as a function of steel absorber has been determined with the result that to reduce the b.g. to <10% of the neutrino signals requires 6-7 m of steel between the detector and the target.

If lepton numbers are separately conserved a. will not lead to reaction with hydrogen but will with (2) below.

$$\nu_e + p \to e^+ + N$$

$$\nu_e + N \to e^- + p$$

(1) $\mu^+ \to e^+\nu$. LASL, Stanford, Chicago (original SIN)

(2) $\mu \to e$. Yale, U. of PA and LASL

Above experiments should provide an important constraint on gauge theories, especially if for example, in (1), one can measure the angular correlation between the μ-spin and the e momentum, $1 + A_{\cos} \theta_{\hat{\sigma}} \cdot \vec{P}$ where A = ± for V ± A interaction.

4. Other Tests of Conservation Laws

a. Time Reversal Invariance

$\pi^+ + T \rightleftarrows He^3 + \gamma$. UCLA

b. Solar Neutrinos. BNL .

5. Symmetry Laws

a. Weak Component of The N-N Interaction.

Maximum parity violation by the weak interaction makes possible the study of the weak component of the N-N interaction. This experiment involves use of longitudinal polarized protons on an unpolarized target. Asymmetries in the transmitted beam resulting from spin reversal would identify a term in the cross section proportional to $\hat{\sigma} \cdot \vec{p}$ where $\hat{\sigma}$ is the proton spin and $\vec{p}$ is its momentum. Drs. Nagle, Frauenfelder and Vincent Yuan are involved in this experiment. It has been started at low energies and at ZGS and will soon get under way at LAMPF.

b. $\underline{\pi^+ + T \rightarrow He^3 + \gamma}$.

This reaction tests time reversal invariance. Data taking has been completed.

6. <u>π-π Scattering Length at Zero Energy. Figures 35 and 36.</u>

E. <u>Practical Applications</u>

1. <u>Cancer Eye. Figures 37 and 38</u>.
2. Pion Radiotherapy. Figures 39, 40, 41, 42, 43 and 44.

REFERENCES

1. L. Rosen, "The Los Alamos Meson Physics Facility, A New Tool for Basic Research and Practical Applications," Intern. Conf. Peaceful Uses At. Energy, Proc. 4th, Geneva, (1971) Paper Vol. 1, Session 1.11, pp. 21-37.

2. D. E. Nagle, "Linear Accelerators for Protons," Ency. Britannica, 70B, W. Benton, USA (1970).

3. D. E. Nagle, E. A. Knapp, "Steady State Behavior of a Ring or of a Chain of Coupled Circuits," Conf. on Proton Linear Acc. Yale U., Oct. 1963 p. 171; "Linear Accelerators for Protons: New Developments," Science <u>157</u> (1967) pp. 145.

4. D. C. Hagerman, R. A. Jameson, "The Los Alamos Meson Physics Facility Accelerator," J. Microwave Power <u>3-2</u> (1968) 75.

5. D. C. Hagerman "805-MHz Power Sources for the LAMPF Accelerator," Prod. 1968 Proton Linear Acc. Conf. Brookhaven Natl, Lab. GNL 50120 (1968) 76.

6. D. A. Swenson, et al, "Stabilization of the Drift Tube Linac by Operation in the π/2 Cavity Mode," Proc. Intern. Conf. High Energy Acc., Cambridge, MA, (1967) CEAL-2000, pp. 67.

7. H. S. Butler, et al., "Computer Control of the Los Alamos Linear Accelerator," IEEE Trans. Nucl. Sci. <u>NS-14</u> 3 (1967) pp. 1030.

8. R. A. Jameson, et al, "Full Power Operation of the LAMPF 805 MHz System" Proc. 1970 Proton Linear Acc. Conf. National Acc. Lab., Sept. 28-Oct. 2, (1970) pp. 483.

9. L. Rosen, "Possibilities and Advantages of Using Negative Pions in Radiotherapy," Nucl. Applications, 5, pp. 379-387.

10. L. Rosen, "The Clinton P. Anderson Meson Physics Facility (LAMPF)," Proc. Nat. Acad. Sci, USA Vol. 70, No. 2, pp. 603-610, February 1973.

11. L. Rosen, "Relevance of Particle Accelerators to National Goals," Los Alamos Scientific Laboratory report LA-DC-12430 (March 1971): 1971 Particle Accel. Conf. Chicago, Illinois, Mar. 1-3, 1971.

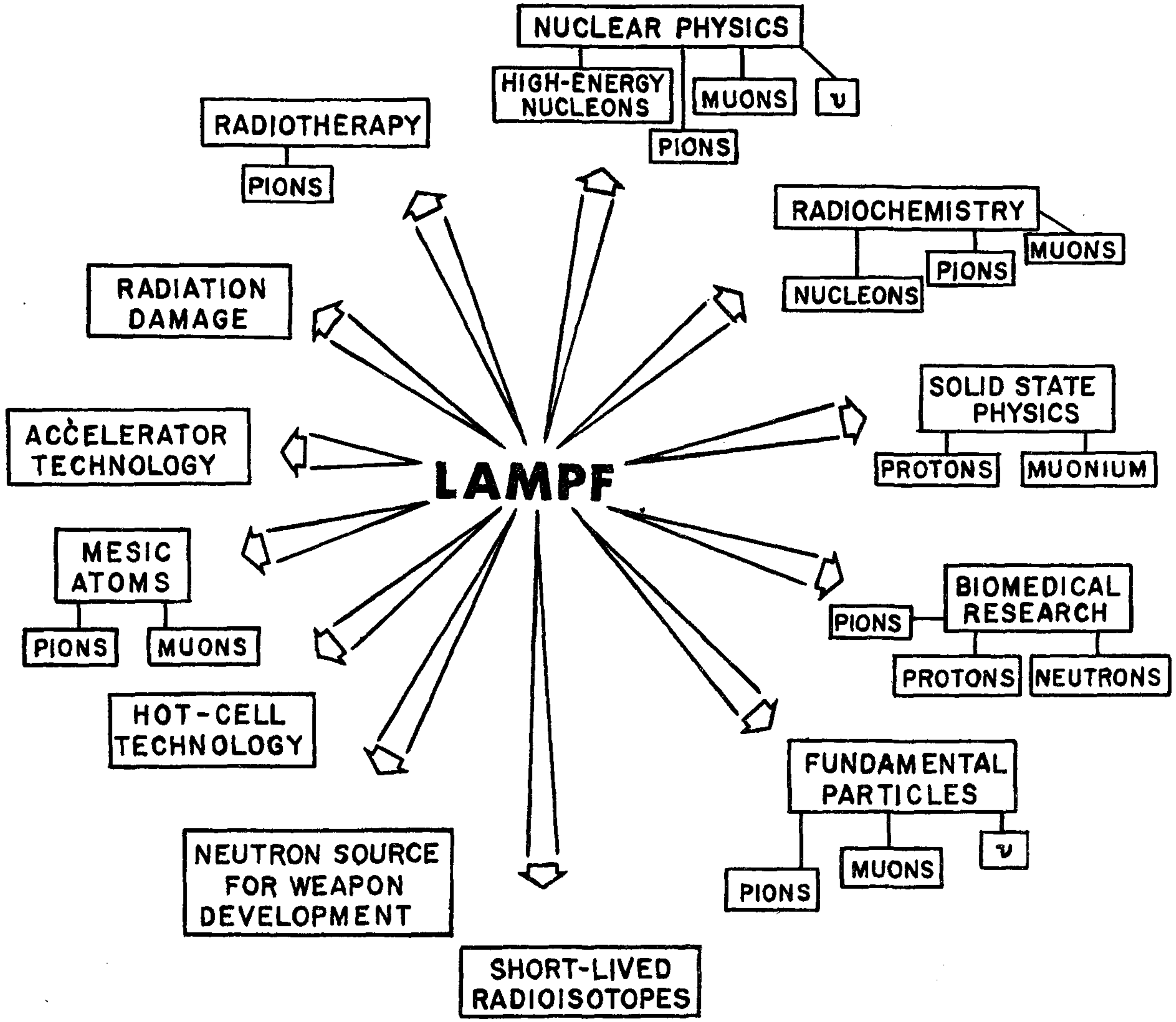

Fig. 1. LAMPF Goals.

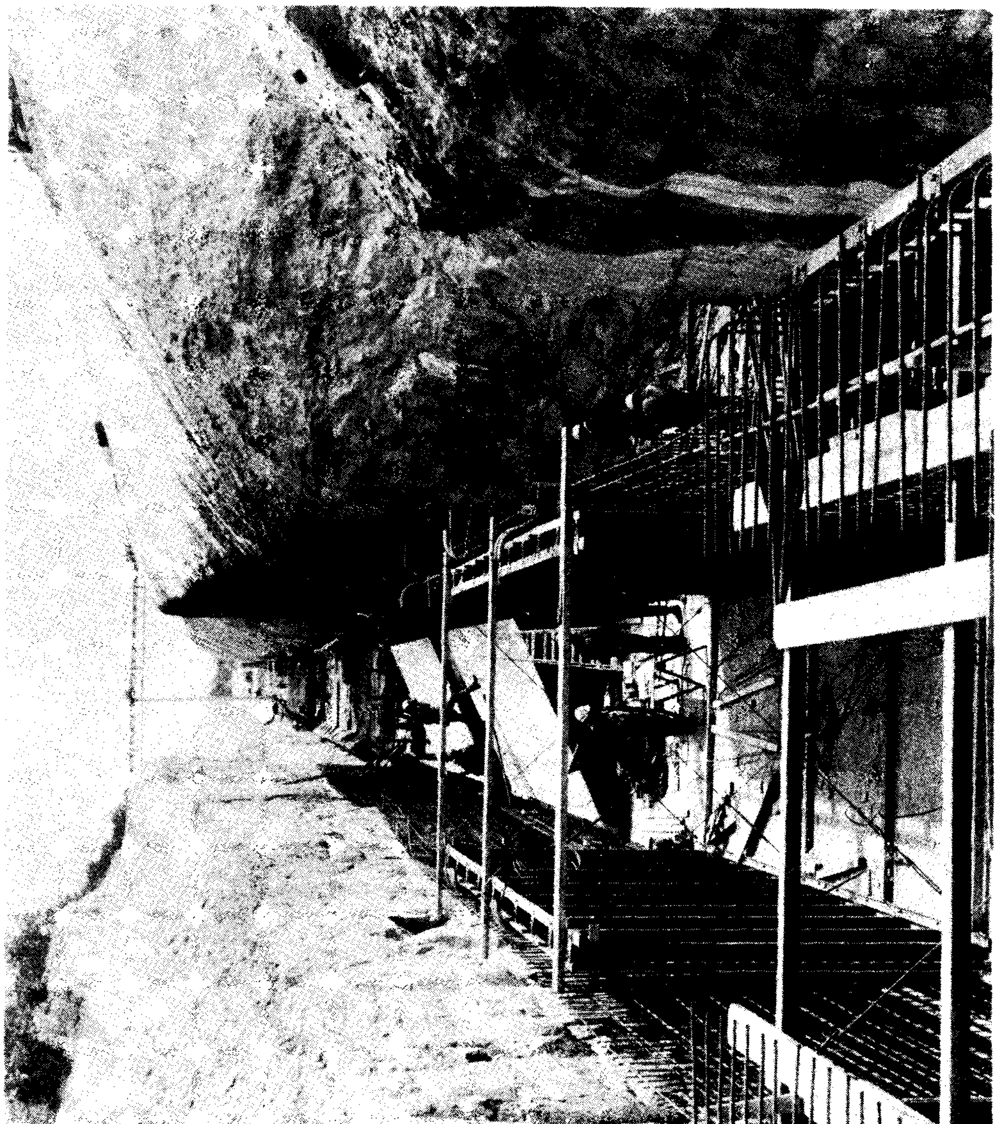

Fig. 2. LAMPF under construction
March 20, 1969.

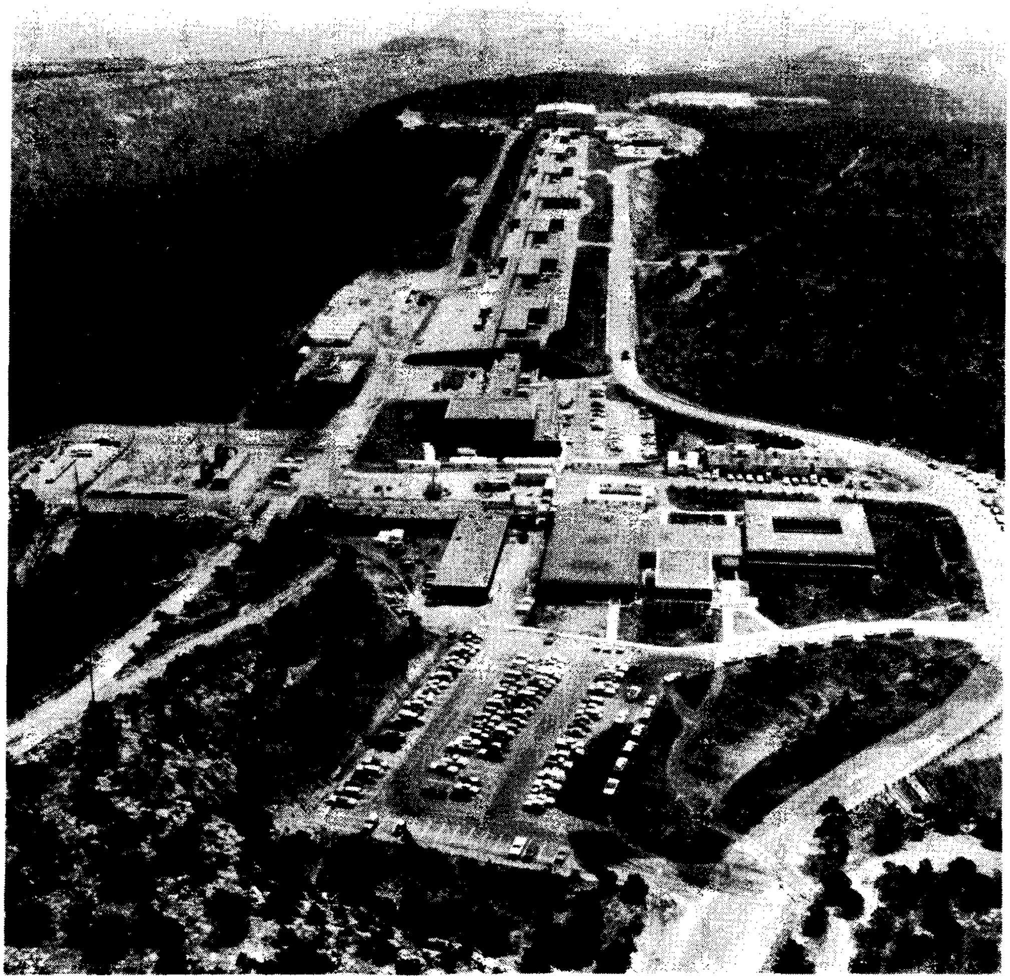

Fig. 2a. LAMPF today.

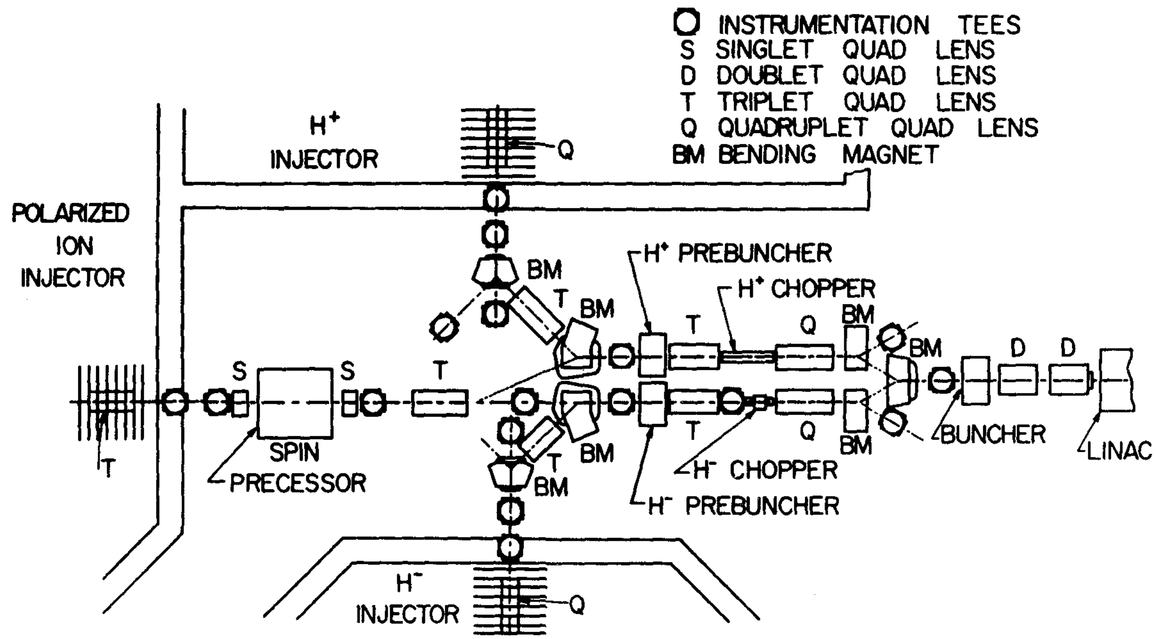

Fig. 3. Schematic of the injector complex.

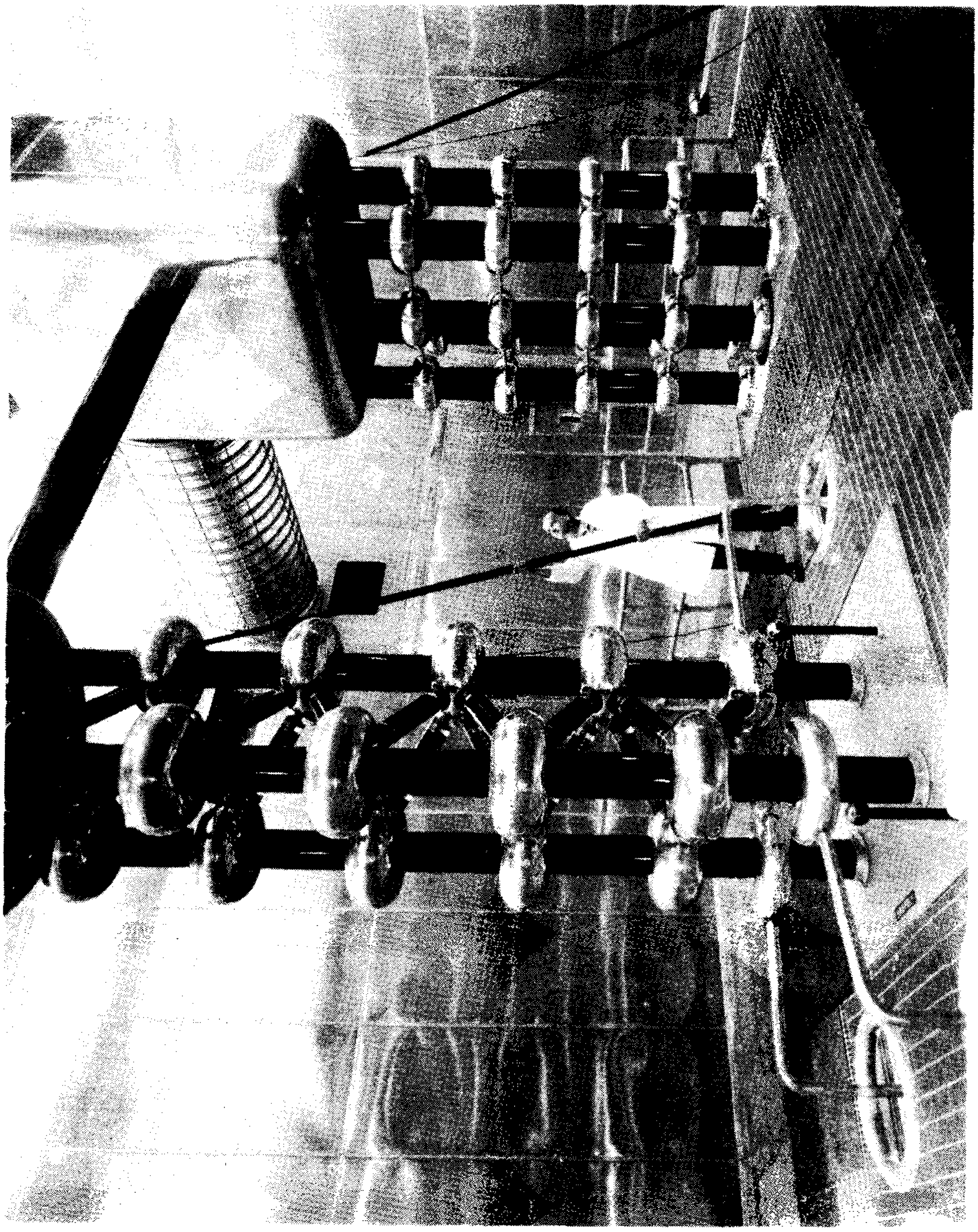

Fig. 4. First Cockcroft-Walton generator installed in its Faraday cage at LAMPF.

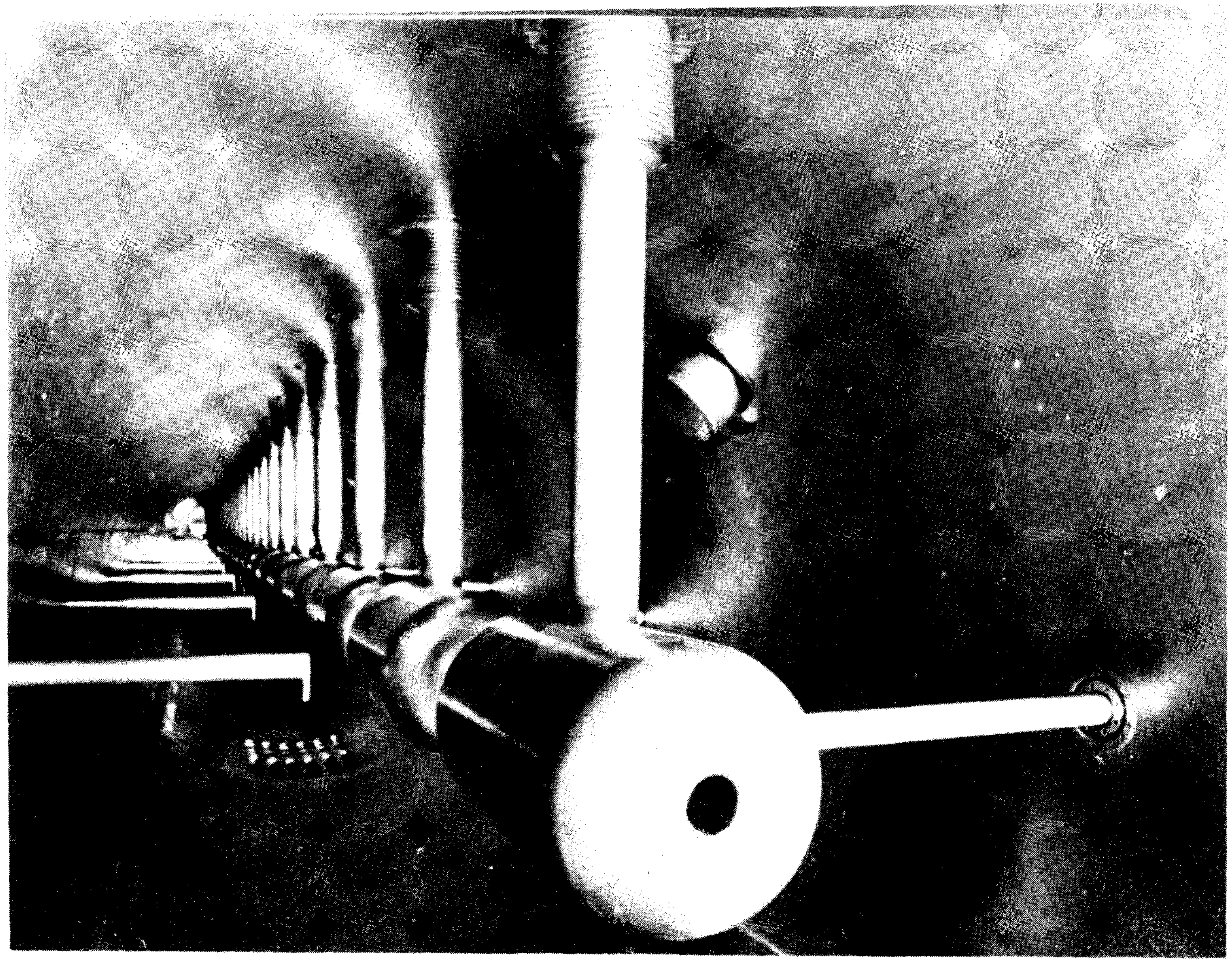

Fig. 5. The Alvarez or drift-tube section.

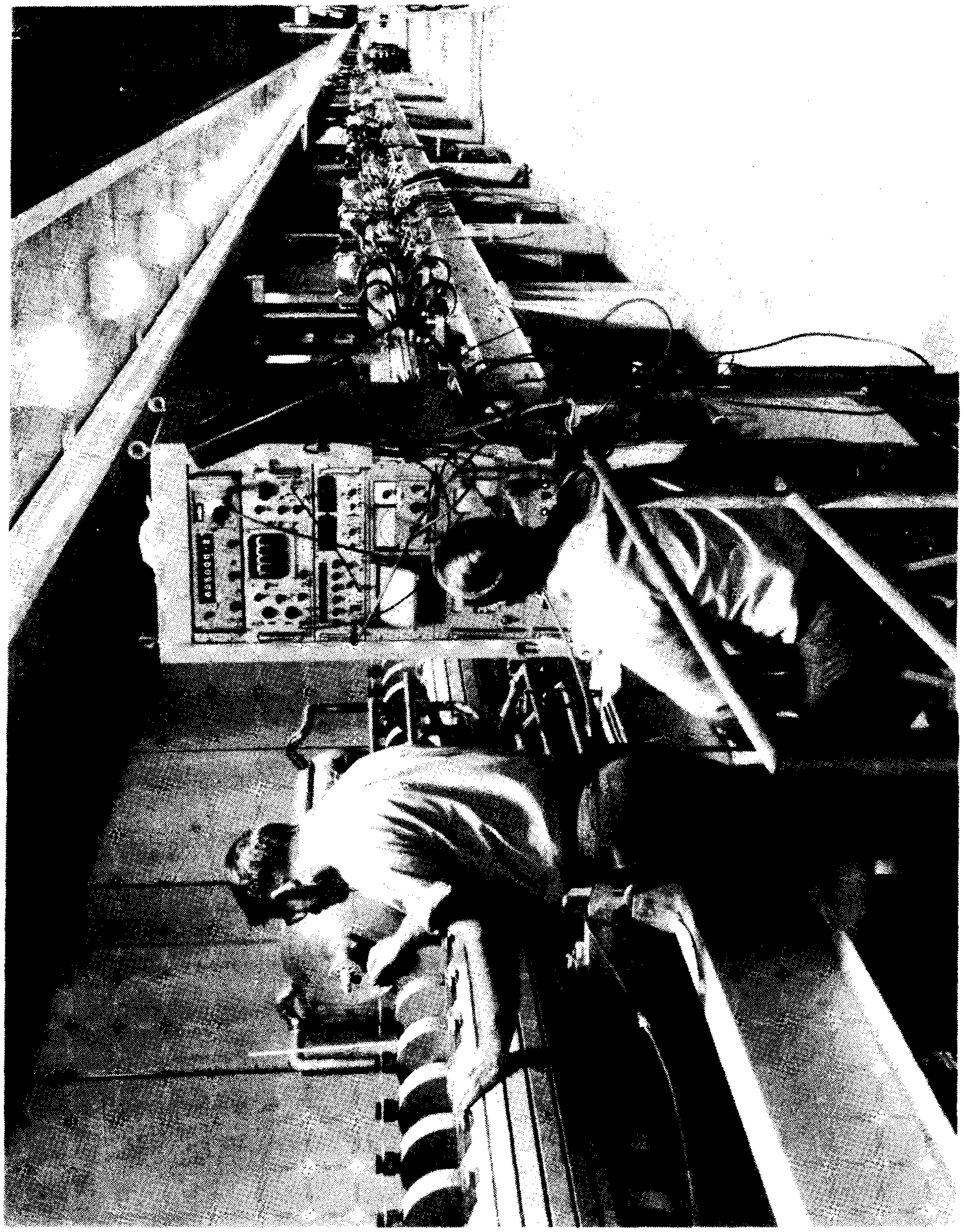

Fig.6 Third stage of the 800-MeV
Proton Accelerator at LAMPF.

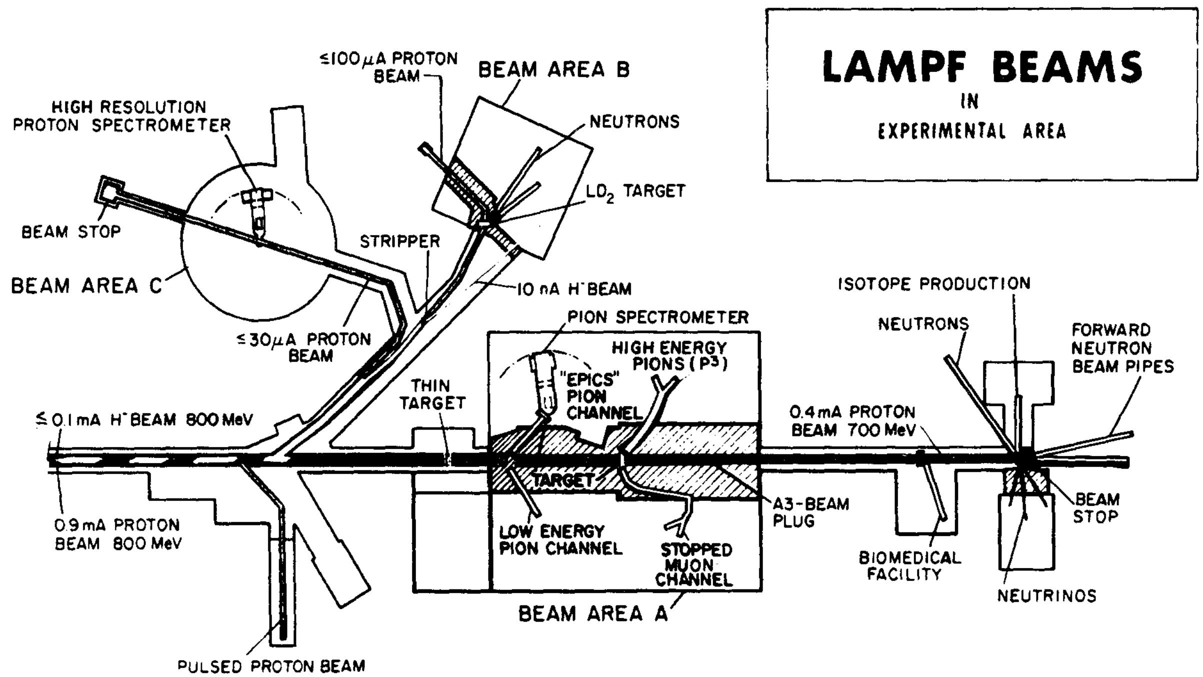

CHANNEL	ENERGY (MeV)	BEAM
LOW ENERGY PION	0-300	$3\times10^9\pi^+/s$ OR $8\times10^8\pi^-/s$
HIGH ENERGY PION (P^3)	100-600	$10^{10}\pi^+/s$ OR $10^9\pi^-/s$
EPICS PION BEAM	50-300	$4\times10^8\pi^+/s$ OR $10^8\pi^-/s$
STOPPED MUON	0-165	$5\times10^7\mu^+/s$ OR $10^7\mu^-/s$

CHANNEL	ENERGY(MeV)	BEAM
NEUTRONS (AREA B)	795	10^7 n/cm^2-s
NEUTRONS (BEAM STOP)	1-20	10^9 n/cm^2-s
BIOMEDICAL	80-100	$2\times10^8\pi^-/s$
NEUTRINOS	20-50	$5\times10^7\nu$/cm^2-s

CHANNEL INTENSITIES QUOTED ABOVE ARE FULL OPEN RATES AT MAXIMUM PROTON CURRENT AND TARGET THICKNESS.

Fig. 7. LAMPF switchyard and experimental areas.

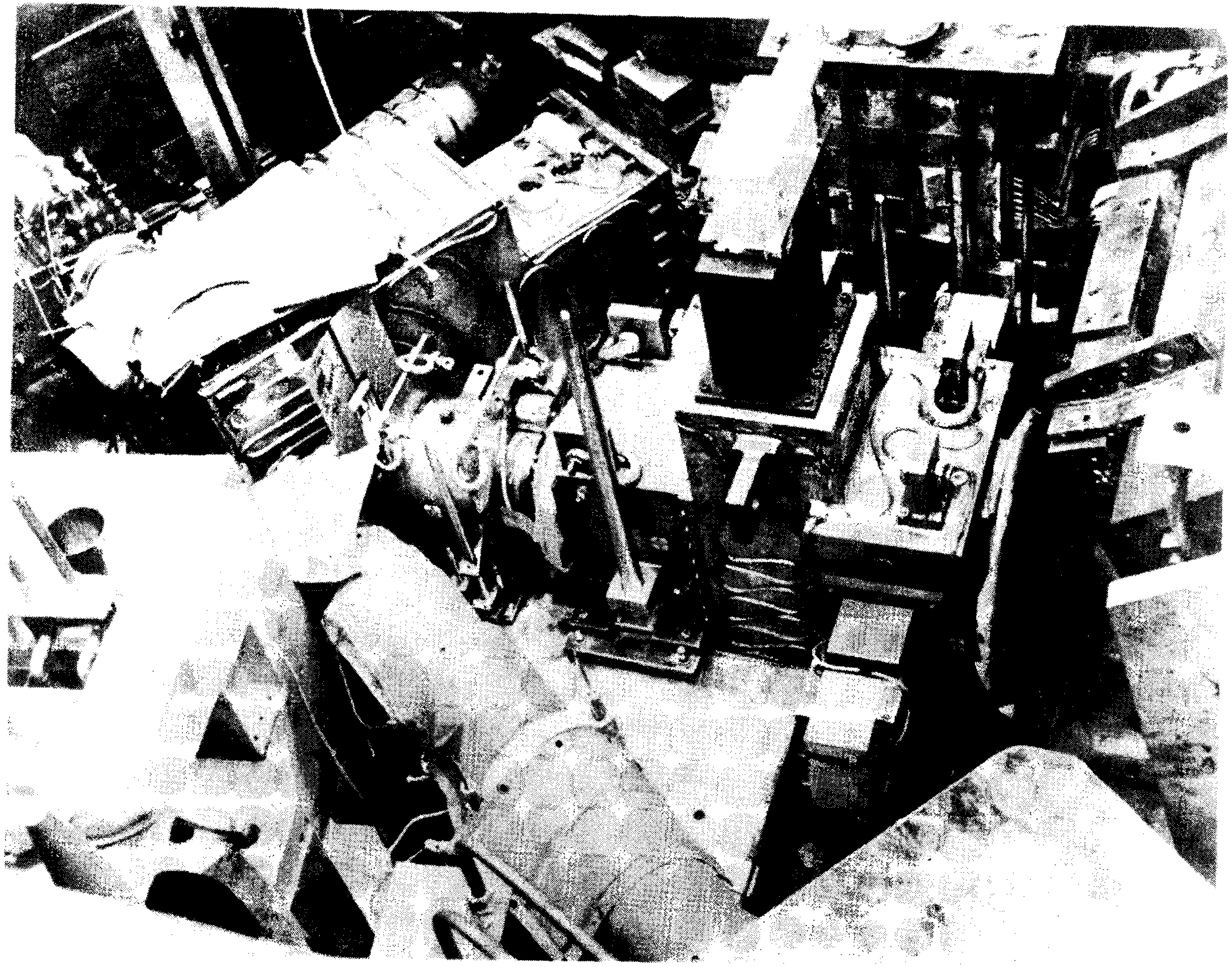

Fig. 8. Target cell in
Experimental Area A

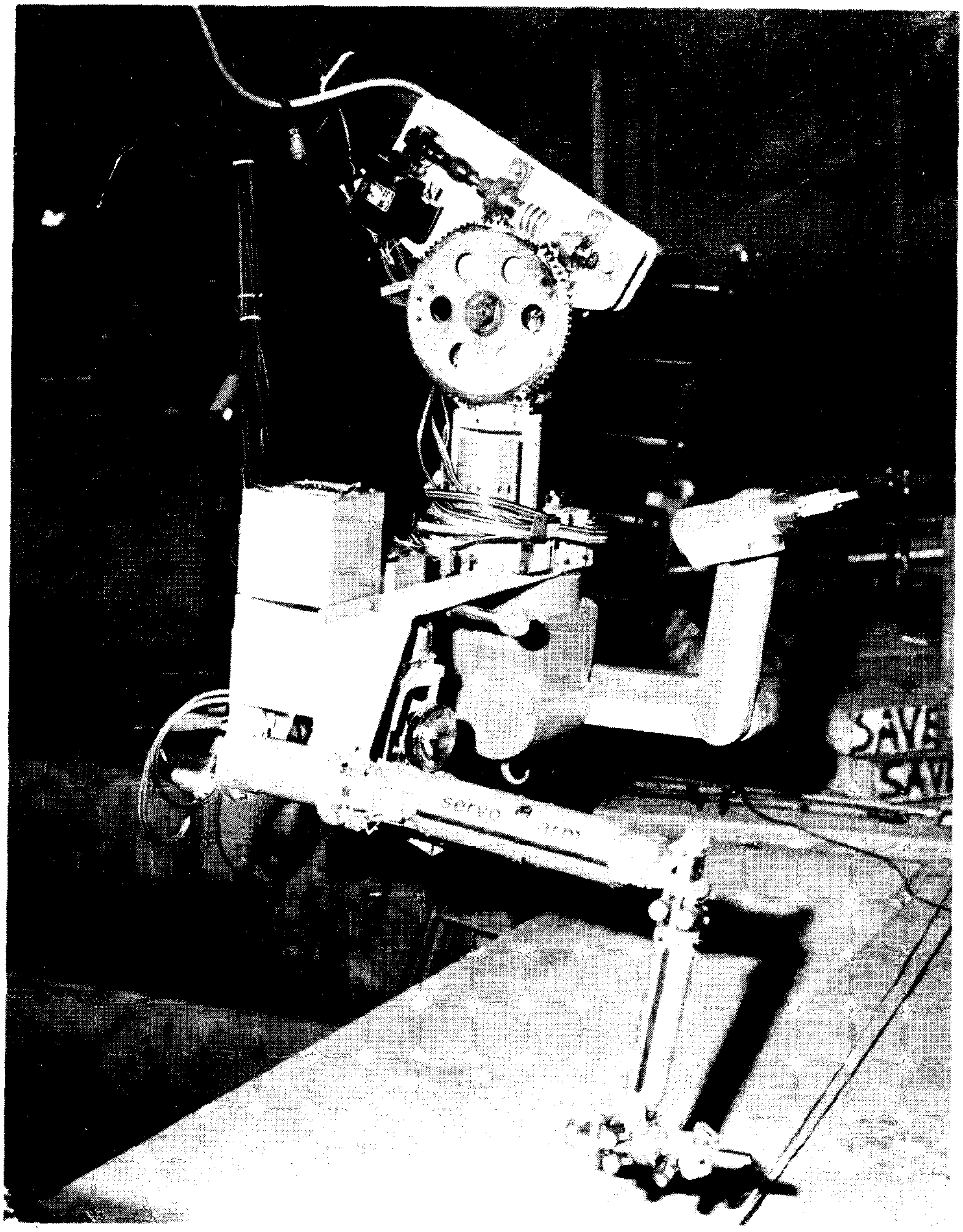

Fig. 8a. Remote manipulator used to service target cells.

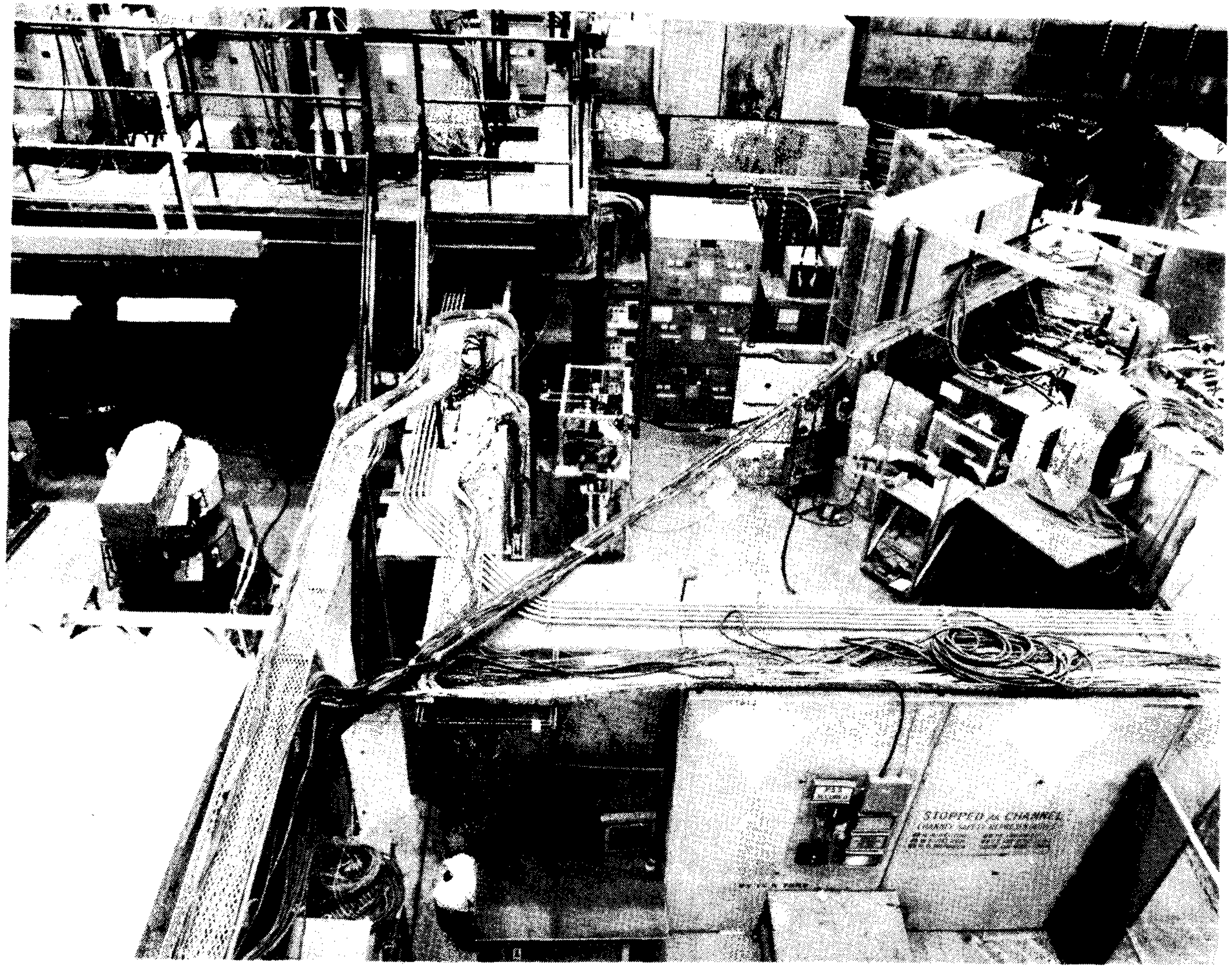

Fig. 9. Stopped Muon Channel in Area A.

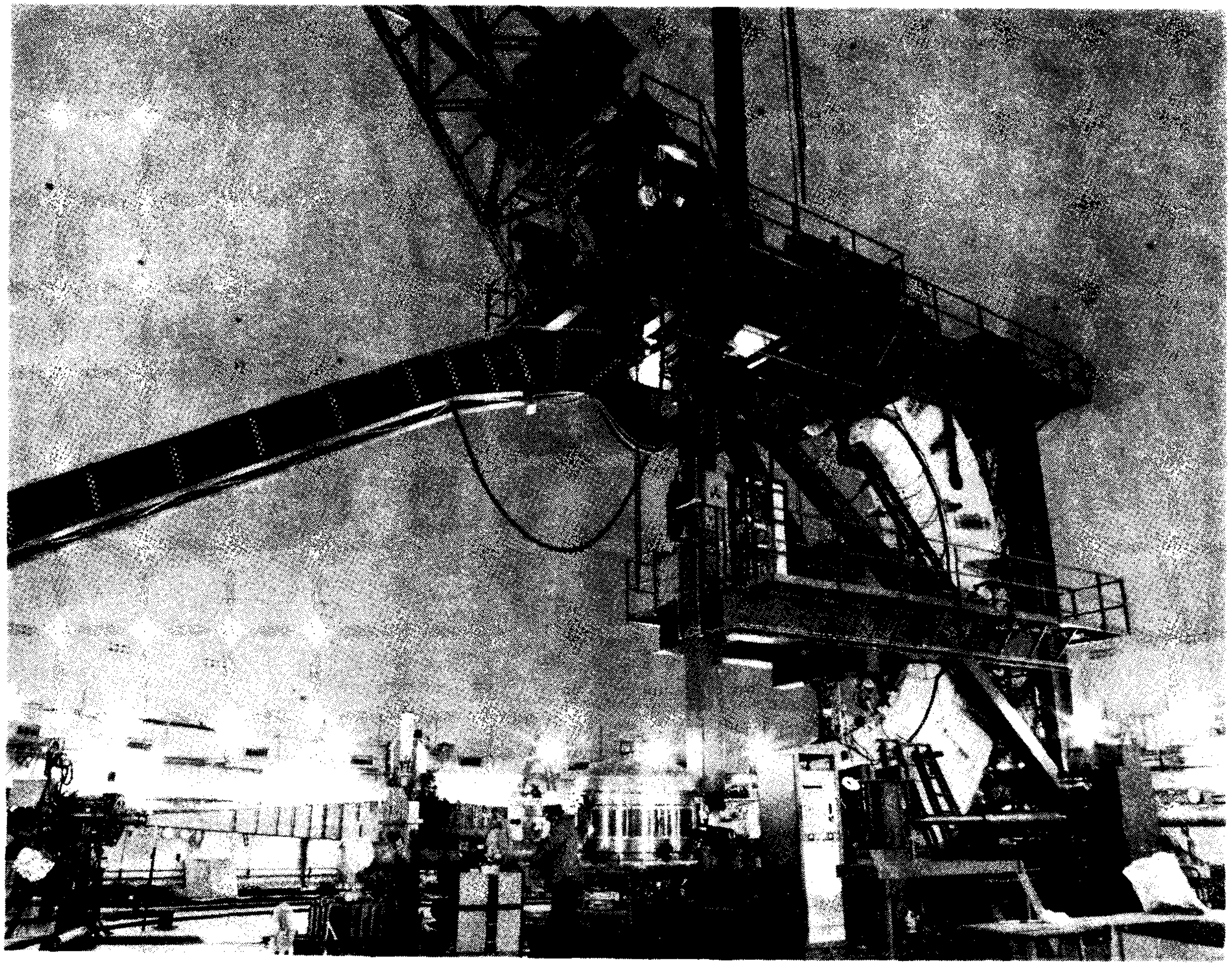

Fig. 10. High Resolution Proton Spectrometer - Area C.

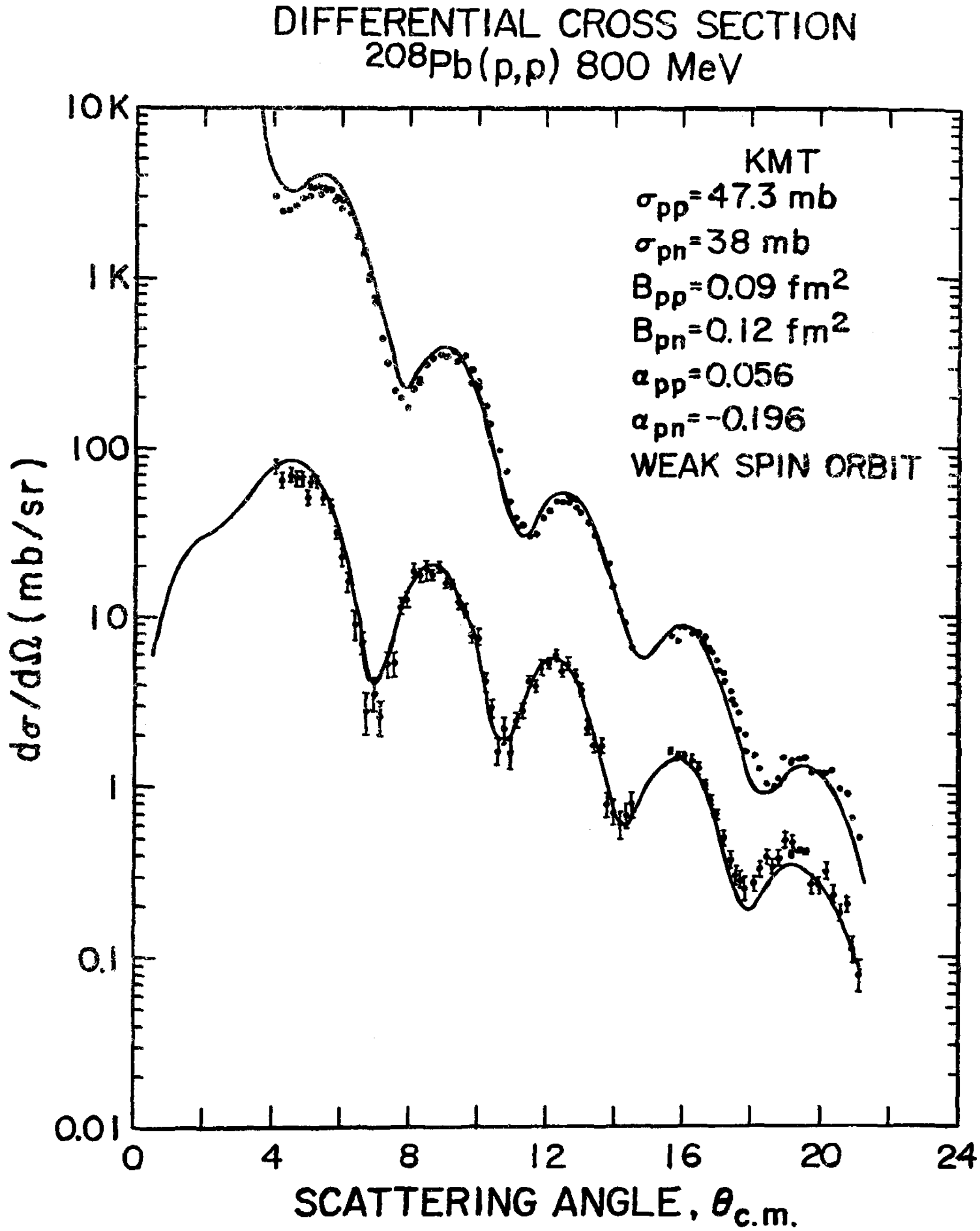

Fig. 10a. Angular distribution of 800 MeV proton elastic scattering from ^{208}Pb.

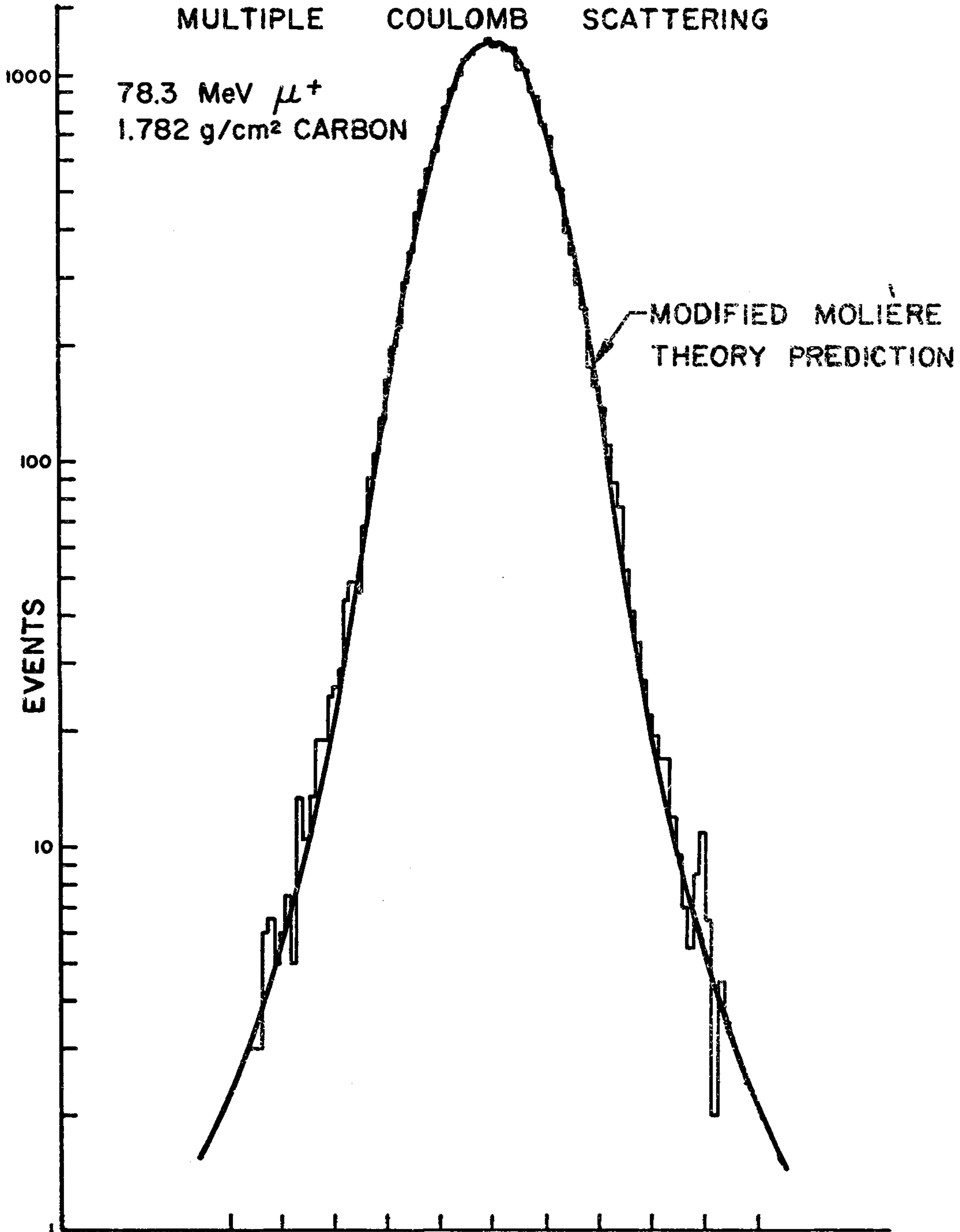

Fig. 11. Multiple Coulomb Scattering

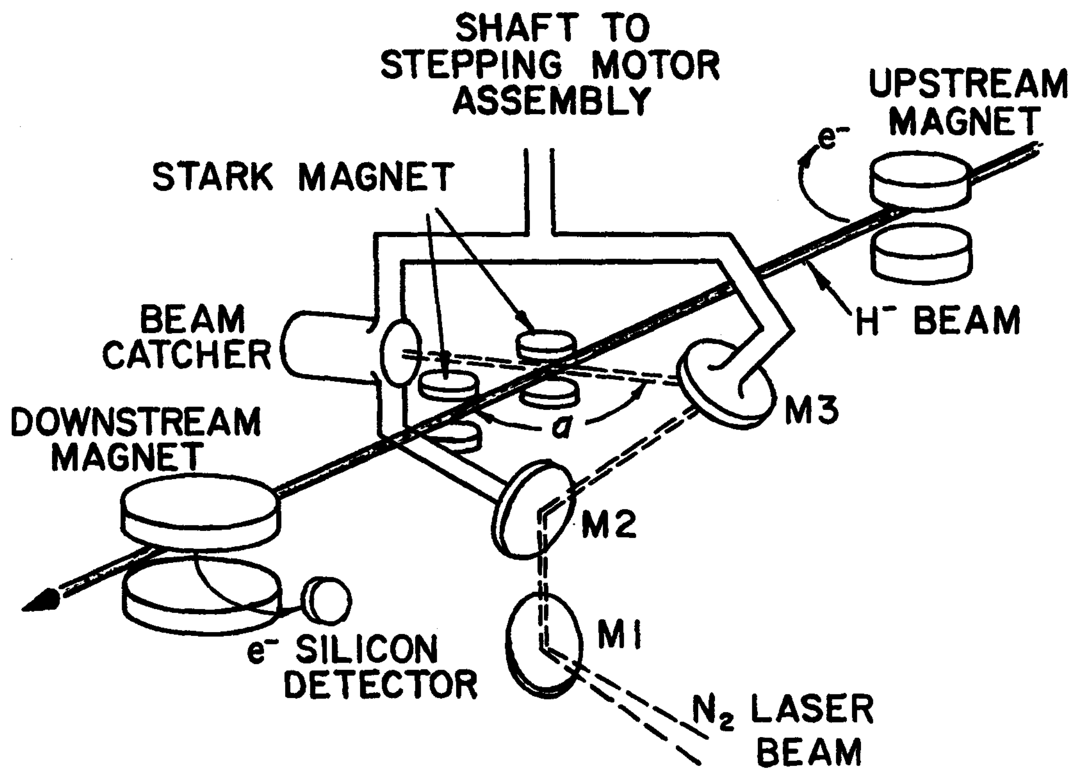

#12. Colliding Beam Experiments
at LAMPF.

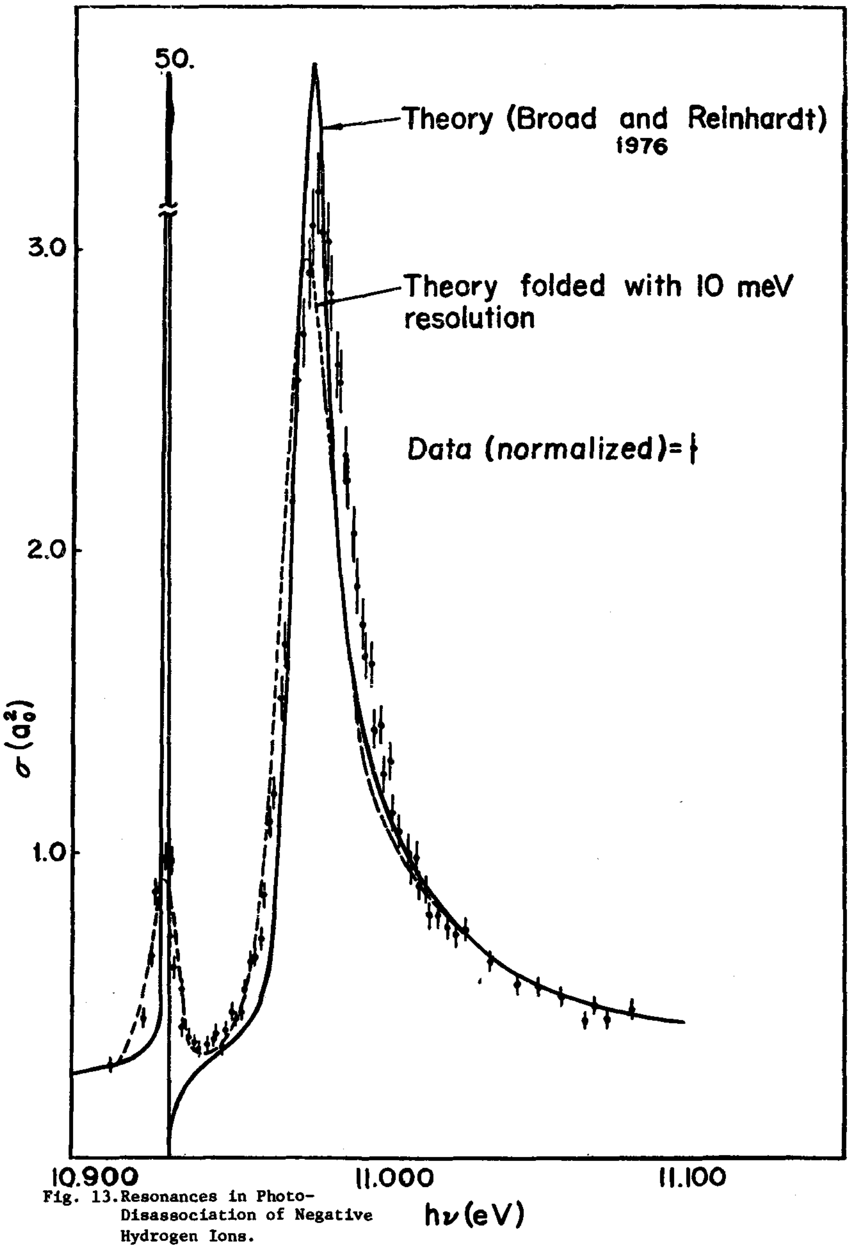

Fig. 13. Resonances in Photo-Disassociation of Negative Hydrogen Ions.

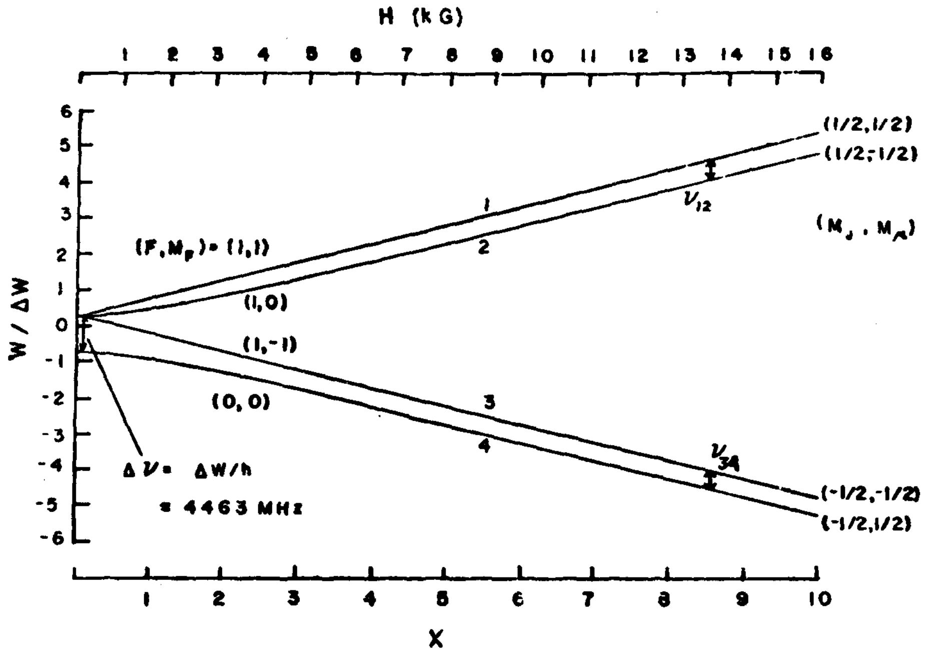

Energy Level Diagram for Muonium in $1^2S_{1/2}$ State

$$\mathcal{H} = a\, \vec{I}_\mu \cdot \vec{J} + \mu_B^e\, g_J\, \vec{J}\cdot\vec{H} - \mu_B^\mu\, g_\mu'\, \vec{I}_\mu\cdot\vec{H}$$

$$x = (g_J\, \mu_B^e + g_\mu'\, \mu_B^\mu)H/(h\Delta\nu)$$

High Field Results:

$\Delta\nu$ = 4 463 302.35 (0.52) kHz (0.12 ppm)

$\Delta\nu$ Theory = 4 463 318.5 (6.5) kHz

μ_μ/μ_p = 3.183 340 3(44) (1.4 ppm)

Fig. 14. Energy Level Diagram for Muonium.

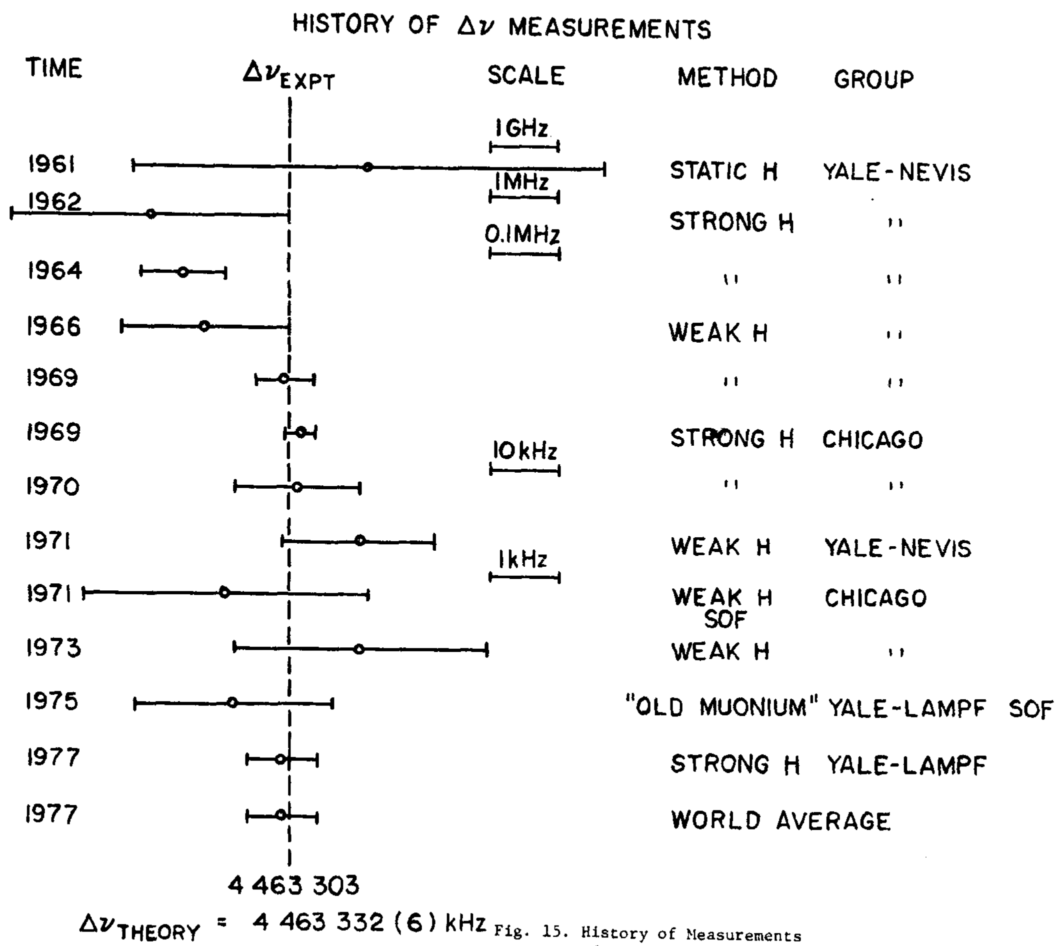

Fig. 15. History of Measurements of Hyperfine Splitting Interval in Muonium

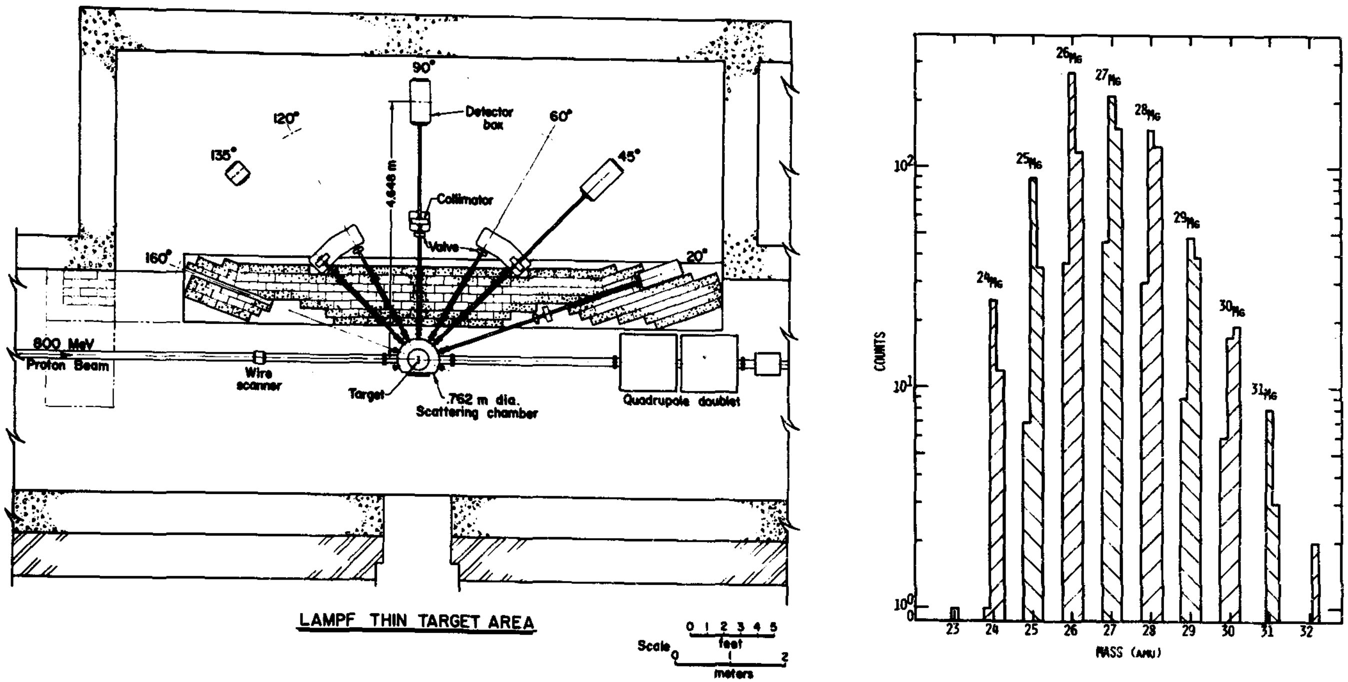

Fig. 16. LAMPF Thin Target Area for Study of Spallation Products.

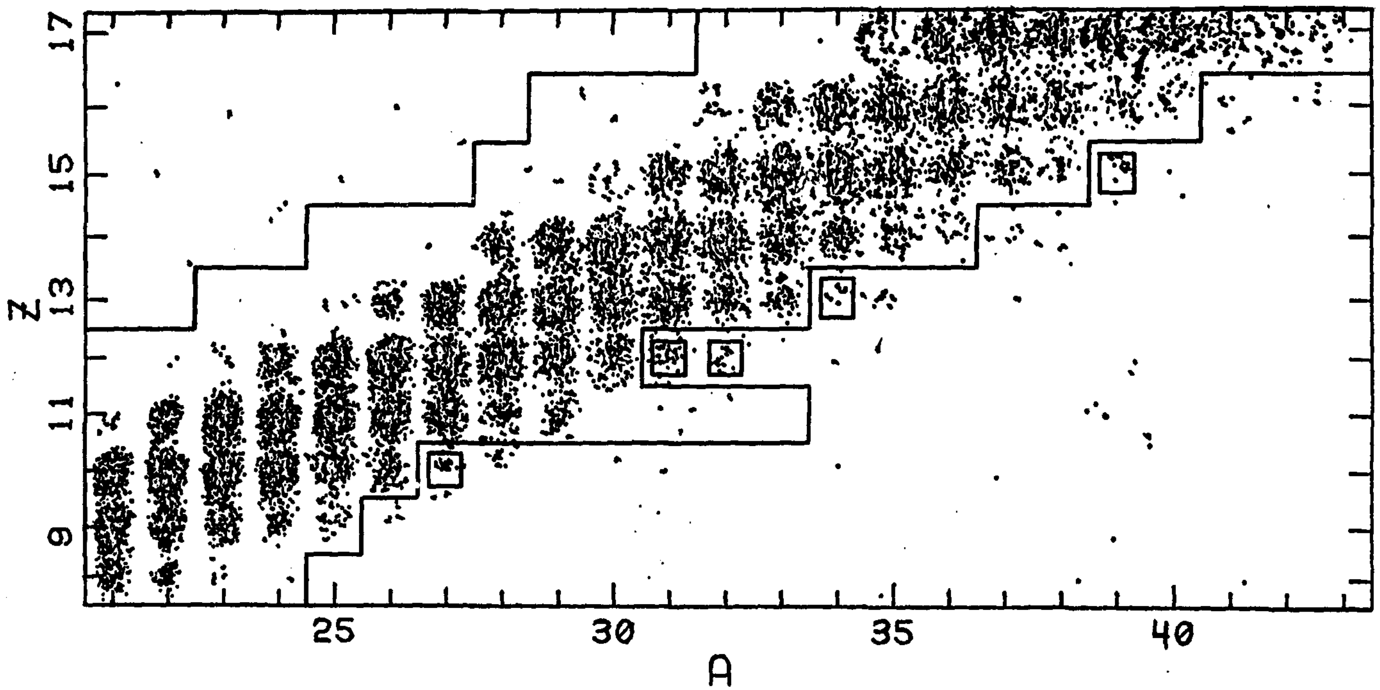

Fig. 17. Mass Distribution for Isotopes of Ne, Mg, Al and p.

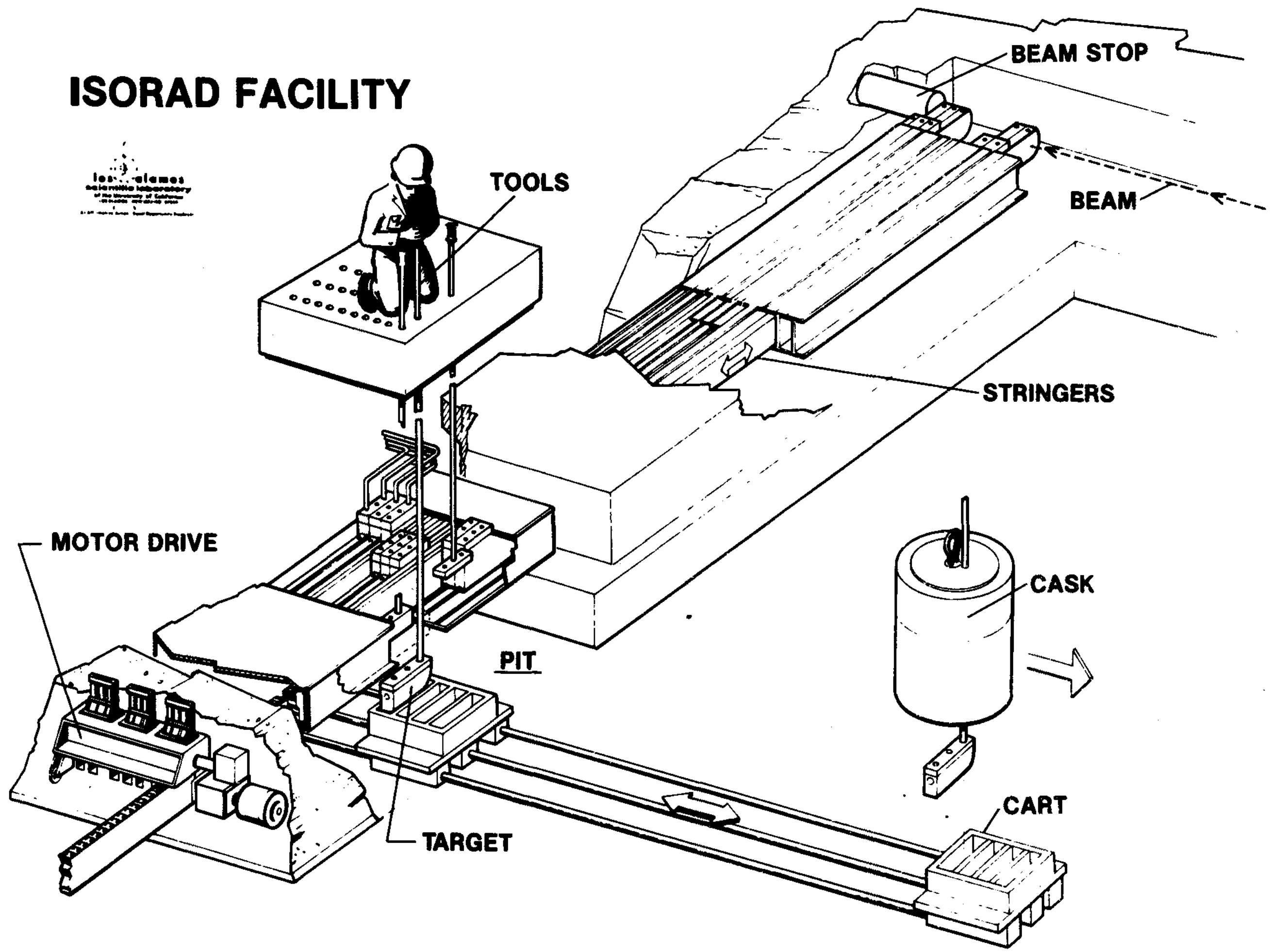

Fig. 18. Isotope Production Facility

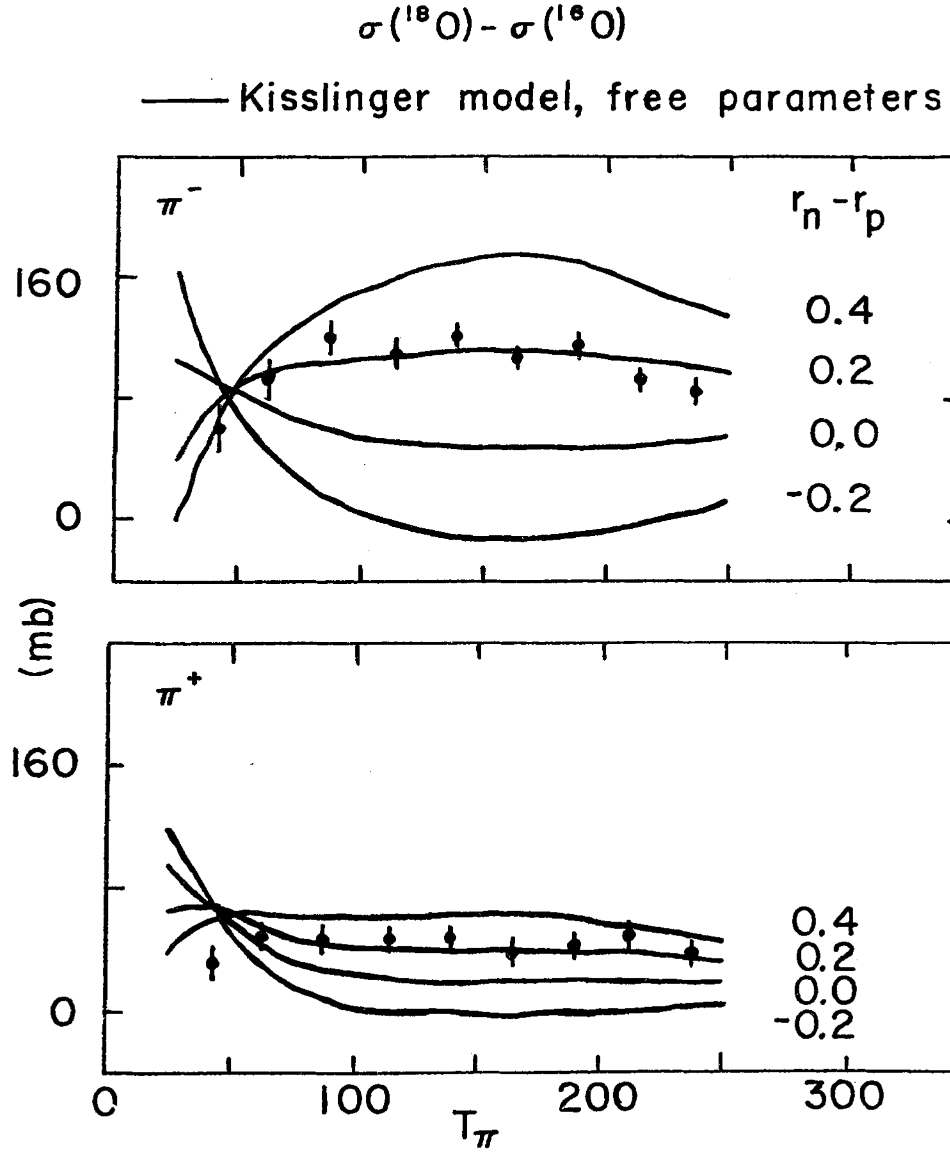

Fig. 19. Energy Dependence of Total Cross Section for $\pi^{\pm}$ on Oxygen Isotopes.

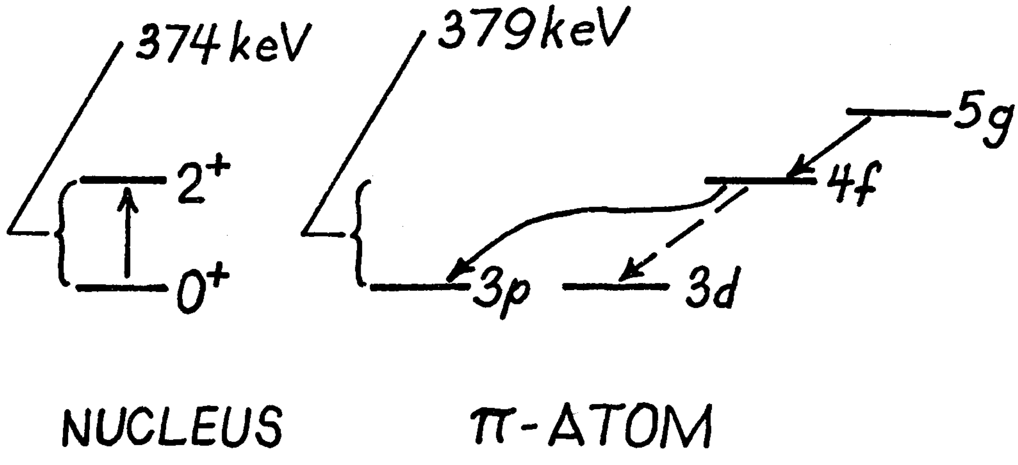

Fig.20. NUCLEAR AND ATOMIC ENERGY LEVELS INVOLVED IN THE NUCLEAR RESONANCE EFFECT IN PIONIC ^{110}Pd.

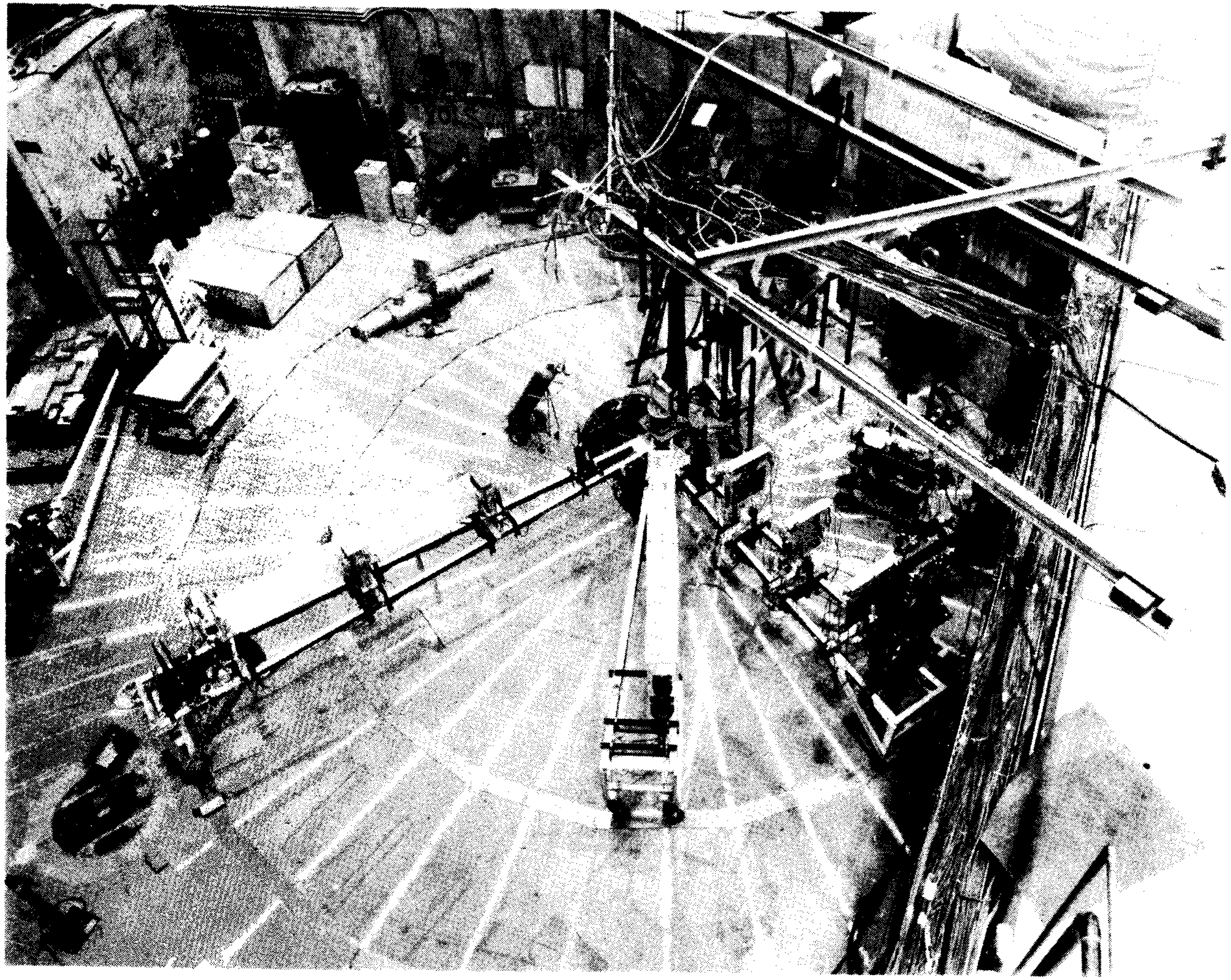

Fig. 21. Layout of instruments for $\pi^+ d \rightarrow pp$ reaction.

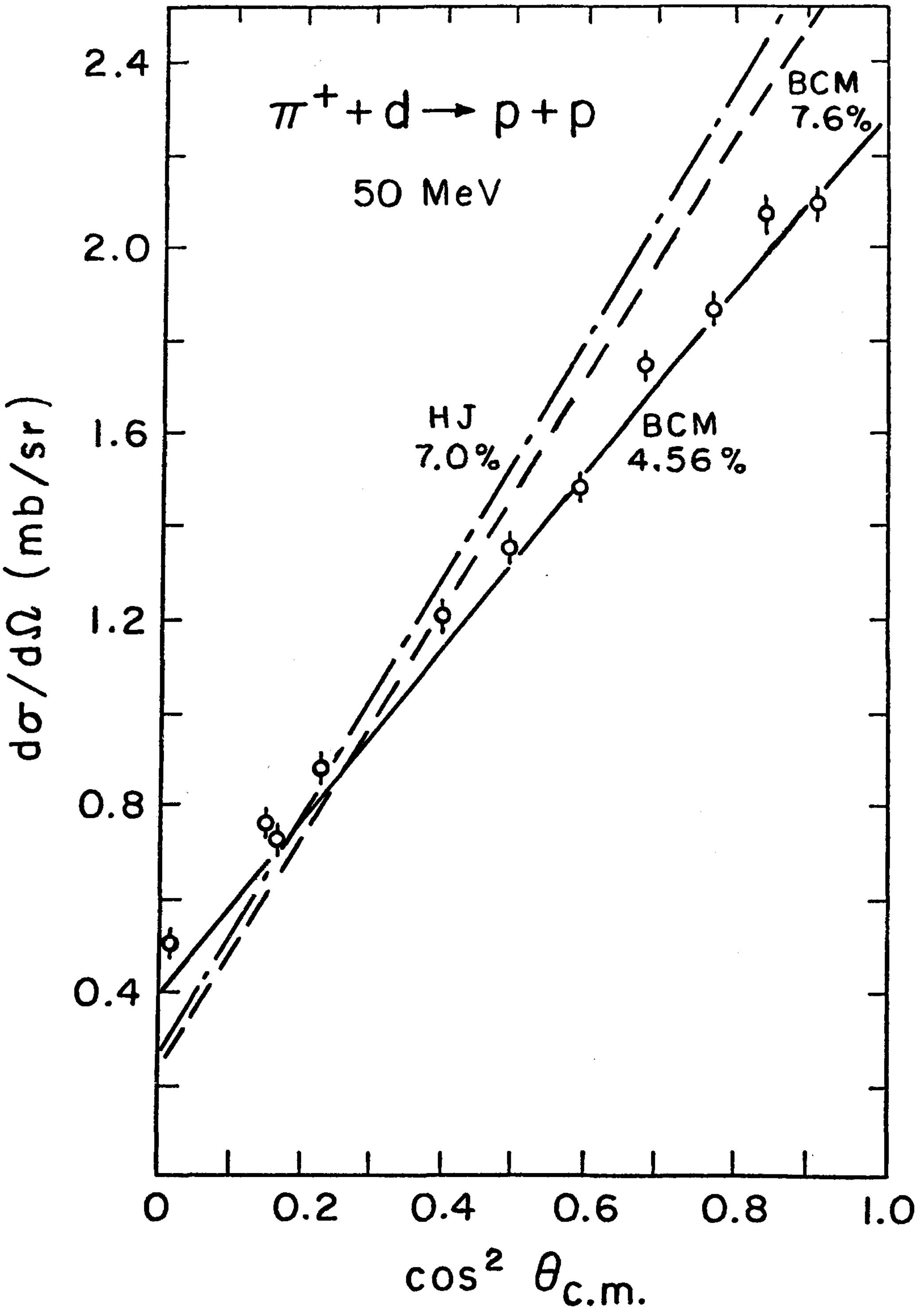

Fig. 22. Differential Cross Section for $\pi^+ d \rightarrow p + p$ at 50 MeV

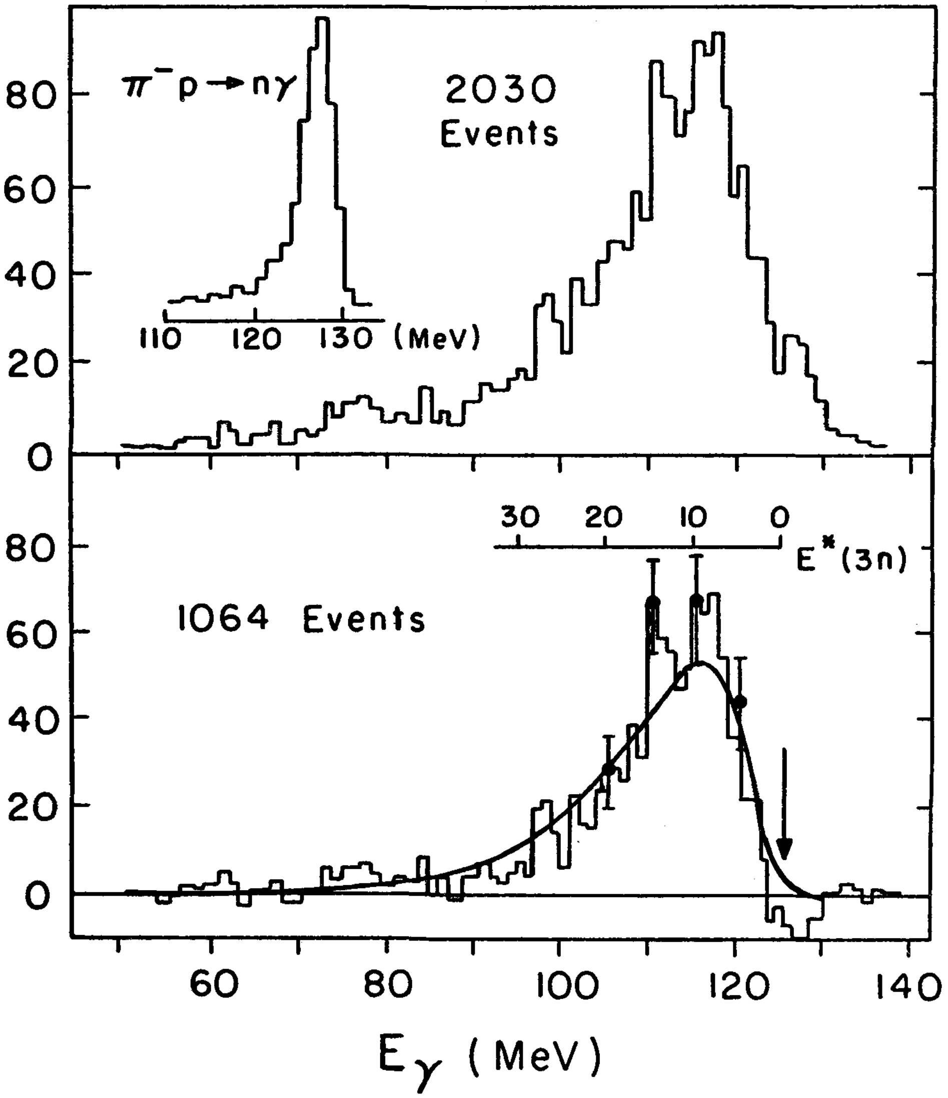

Fig. 23. π^- Capture in Tritium.

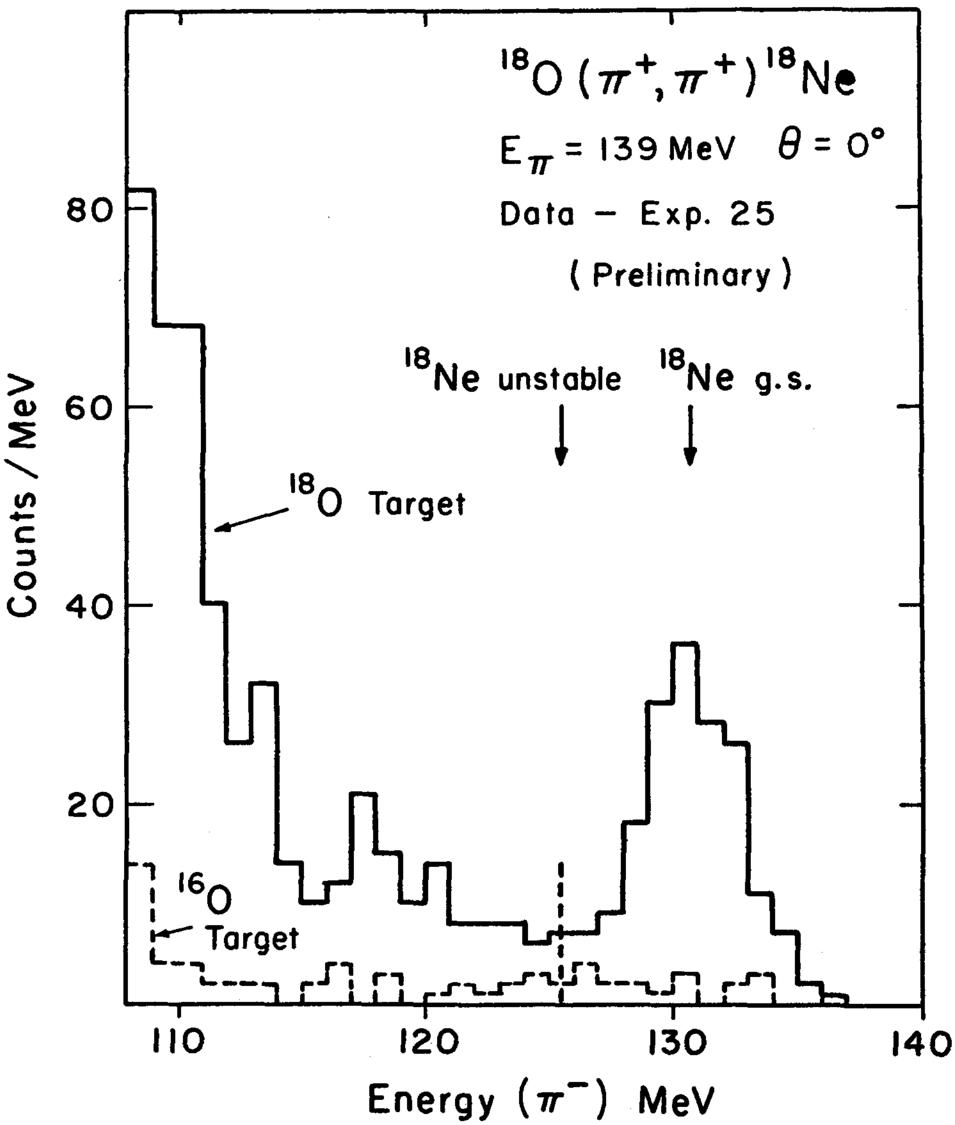

Fig. 24. Pion Double Charge Exchange on O^{18}.

EXPERIMENT #25 - DOUBLE-CHARGE-EXCHANGE
(LASL, UNIV. SOUTH CAROLINA, ANL)

THE (π^+,π^-) REACTION ON A NUCLEUS CHANGES TWO NEUTRONS INTO TWO PROTONS:

$${}_{Z}A_{N} \xrightarrow{(\pi^+,\pi^-)} {}_{Z+2}A_{N-2}$$

THE CROSS-SECTION $d\sigma/d\Omega(0^\circ)$ WAS OBSERVED BY USING A PION CHANNEL AS BOTH A π^+ CHANNEL (1ST HALF) AND A π^- SPECTROMETER (2ND HALF):

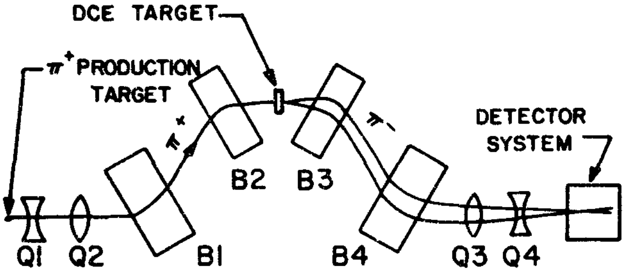

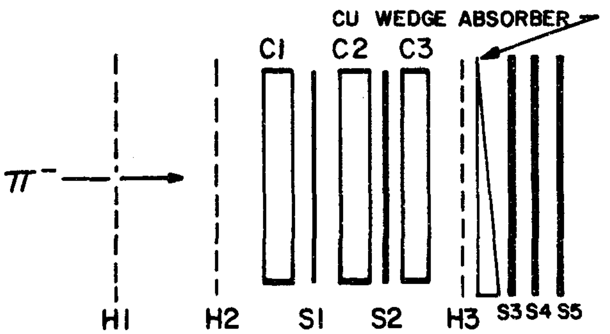

H1-3 HELICAL WIRE CHAMBERS
C1-3 PLASTIC CERENKOV COUNTERS
S1-5 SCINTILLATOR COUNTERS

DETAILS OF DETECTOR SYSTEM

Fig. 25. Experimental Arrangement for Pion Double Charge Exchange.

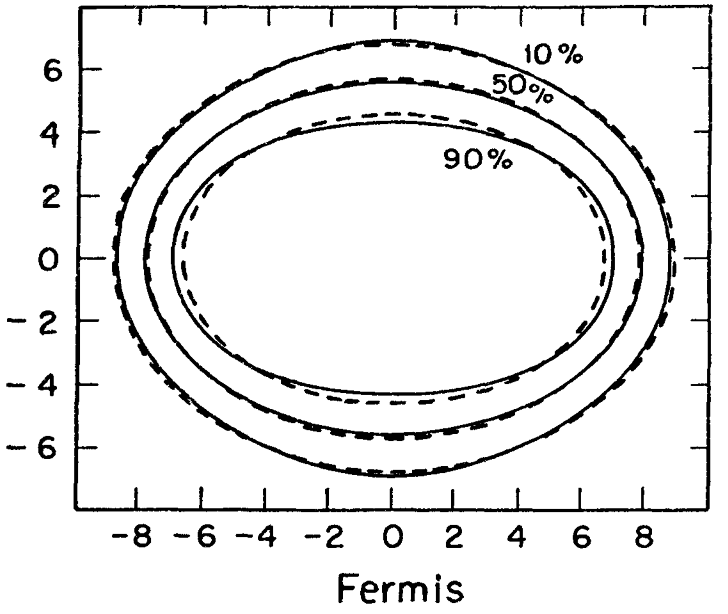

Fig. 26. Charge Distributon in ^{165}H.

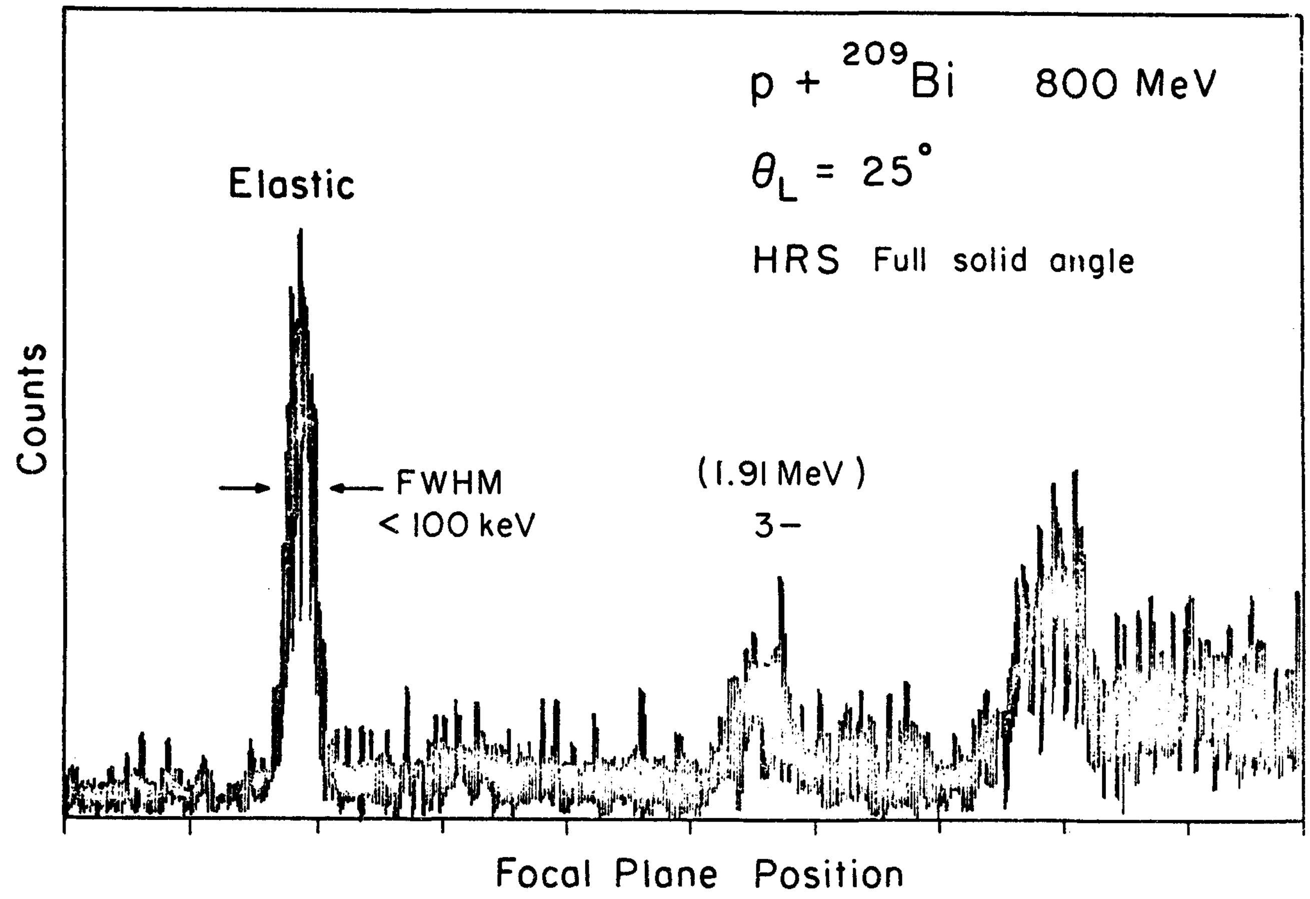

Fig. 27. HRS Resolution

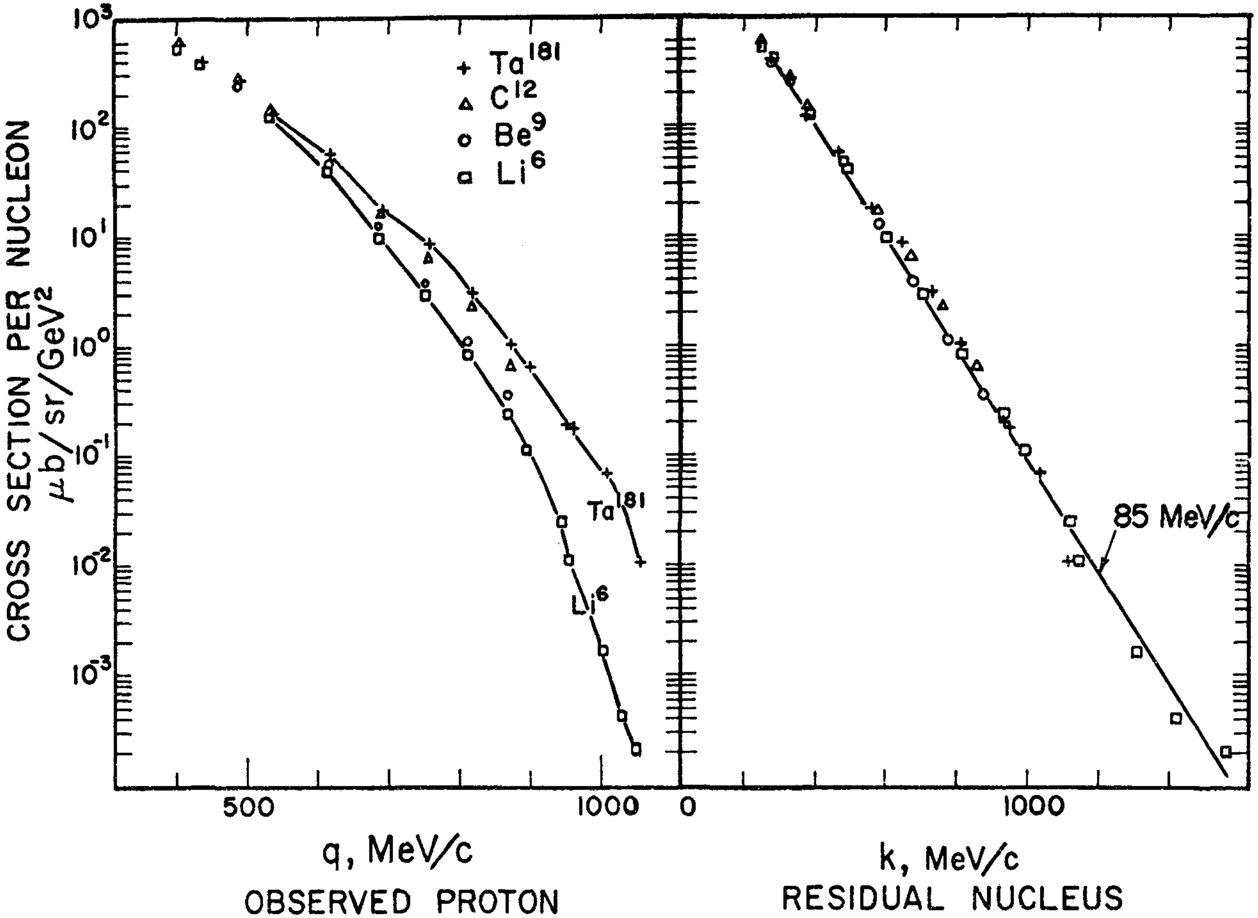

Fig. 28. Large-Angle Scattering of 800 MeV Proton.

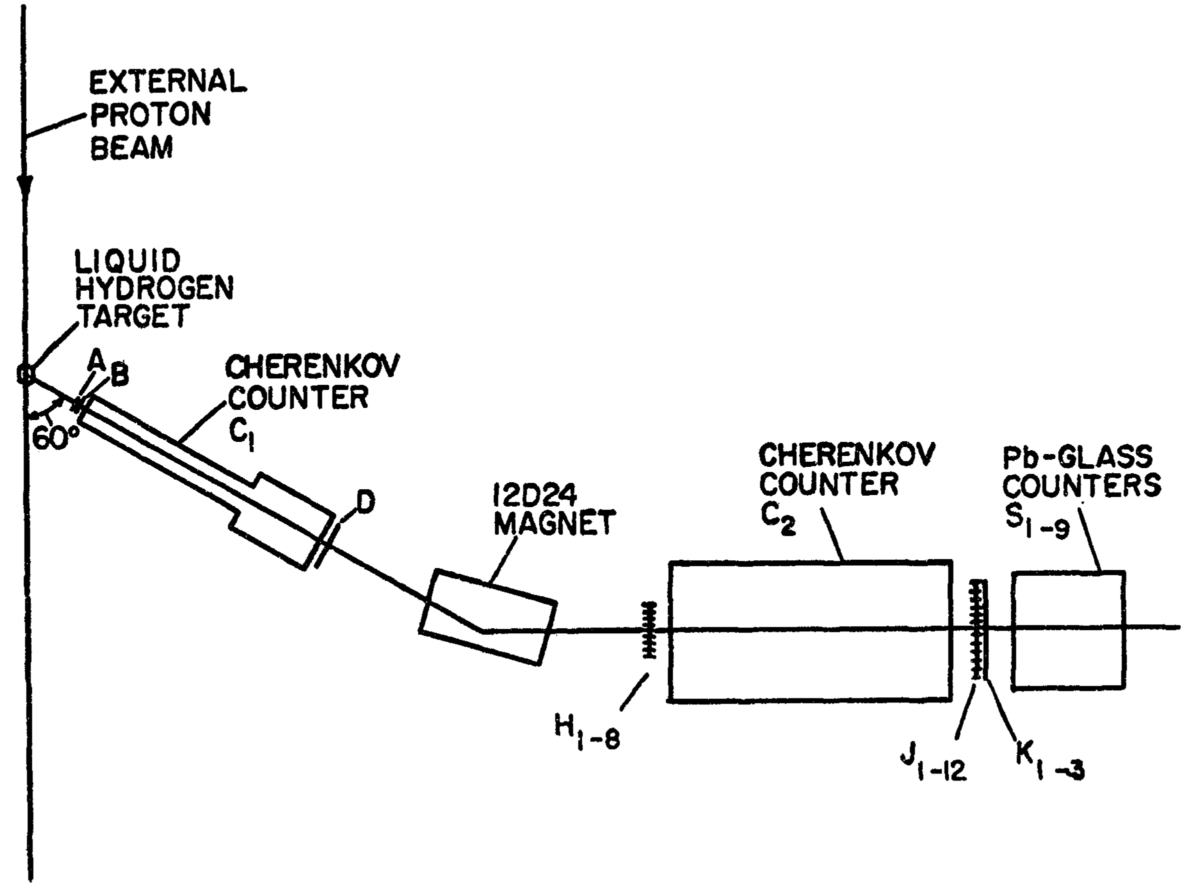

Fig. 29. Experimental Arrangement for Direct Lepton Production Experiment.

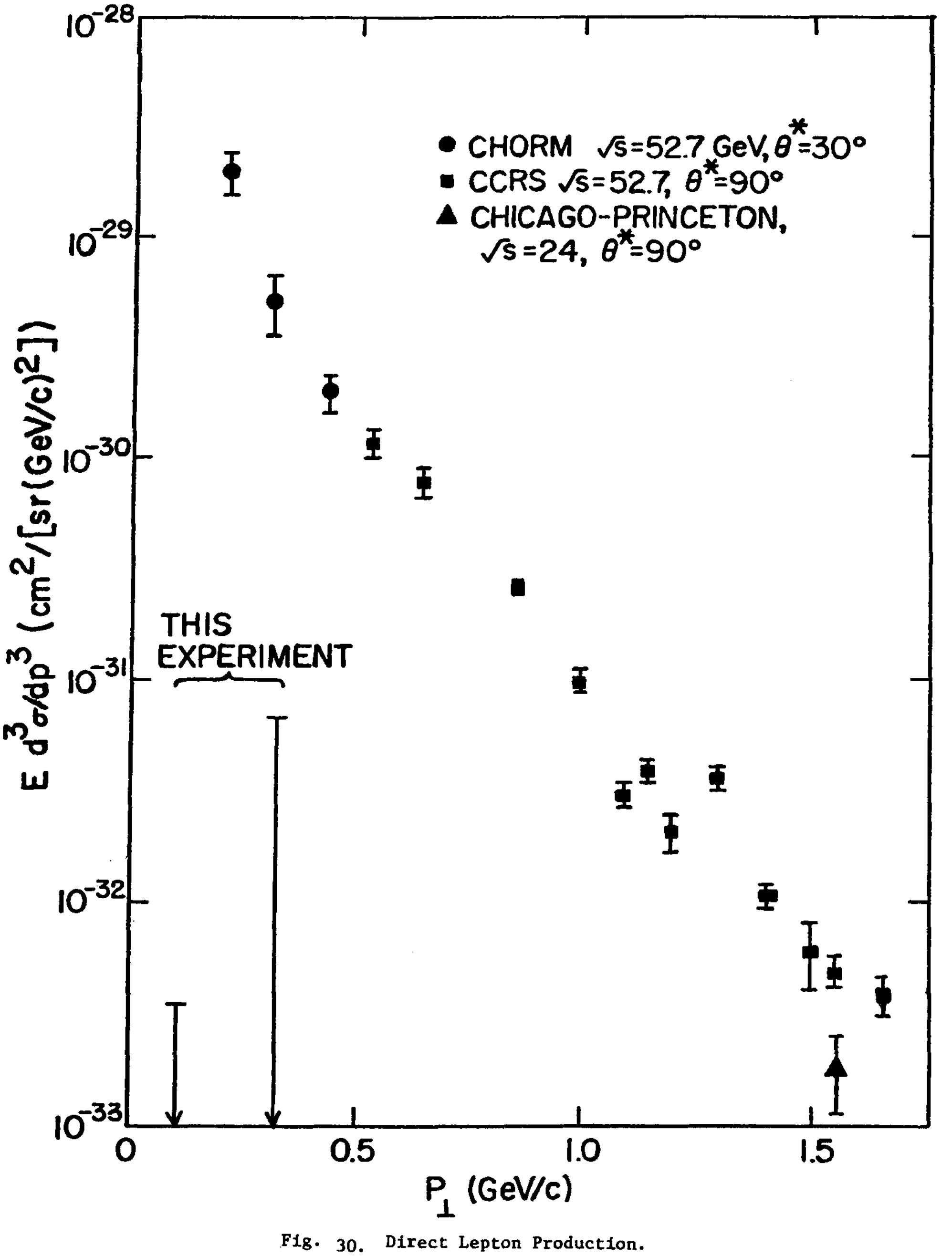

Fig. 30. Direct Lepton Production.

$\pi^0 \to \gamma\gamma\gamma$

C conservation

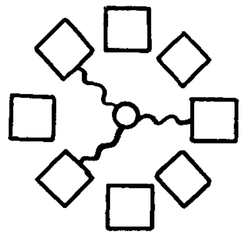

$\pi^0 \to \gamma e^+ e^-$

$$\frac{\Gamma(\pi^0 \to \gamma e^+ e^-)}{\Gamma(\pi^0 \to \gamma\gamma)} = (1.166 \pm 0{,}048) \times 10^{12}$$

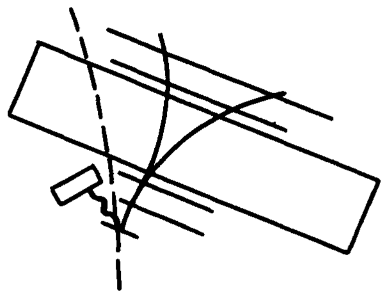

$\pi^0 \to e^+ e^-$

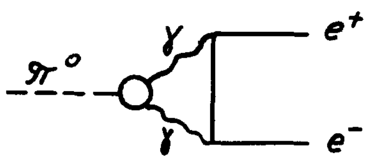

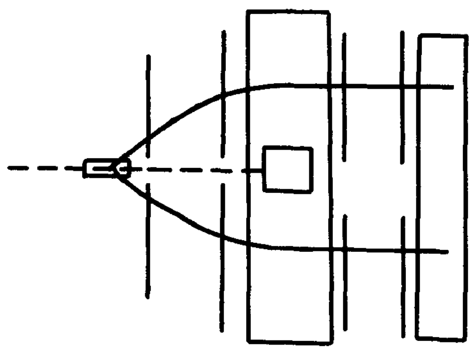

Fig. 31. π^0 Decay Modes Investigated at LAMPF.

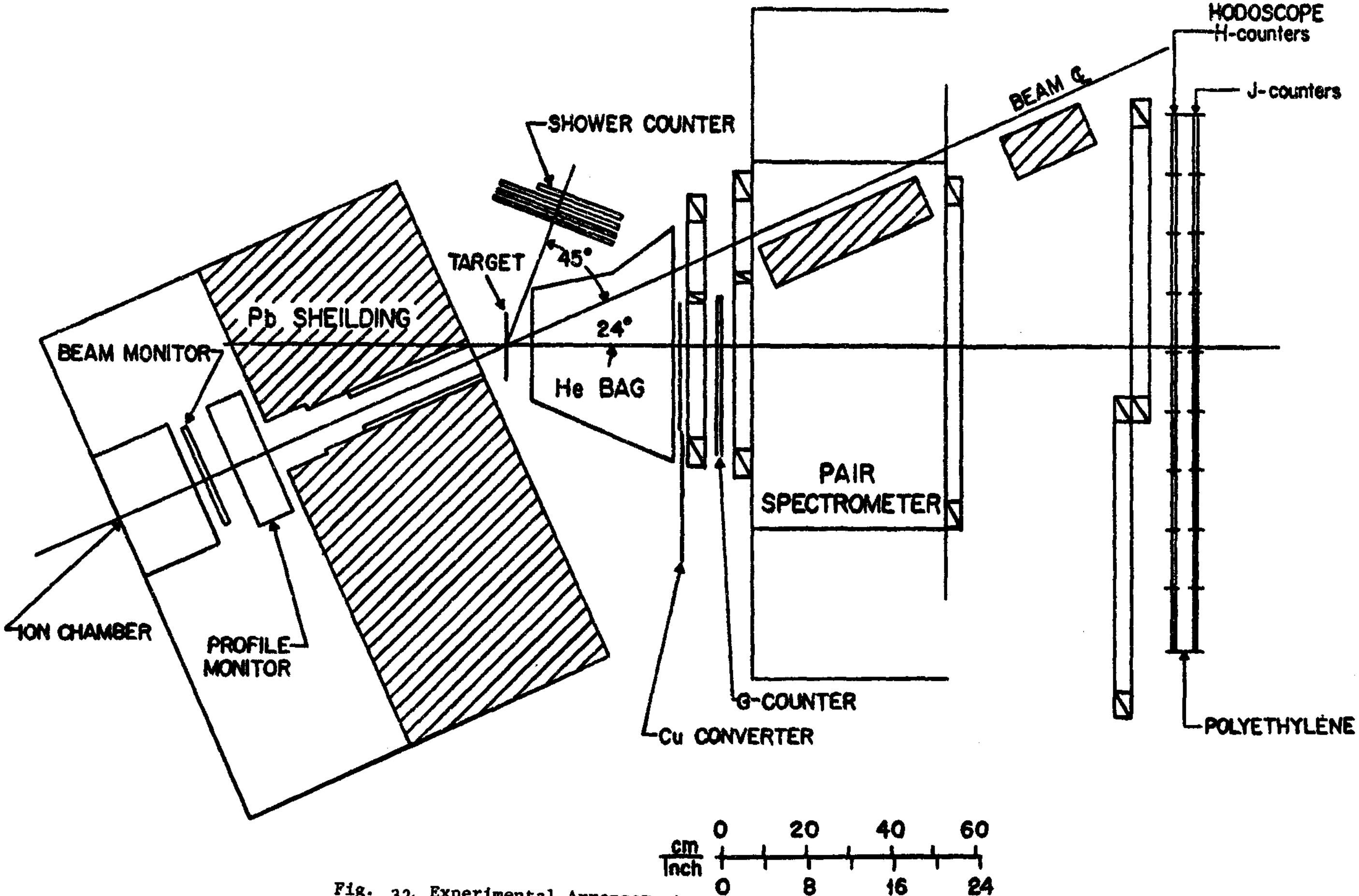

Fig. 32. Experimental Arrangement for Studying π^0 Decay Modes.

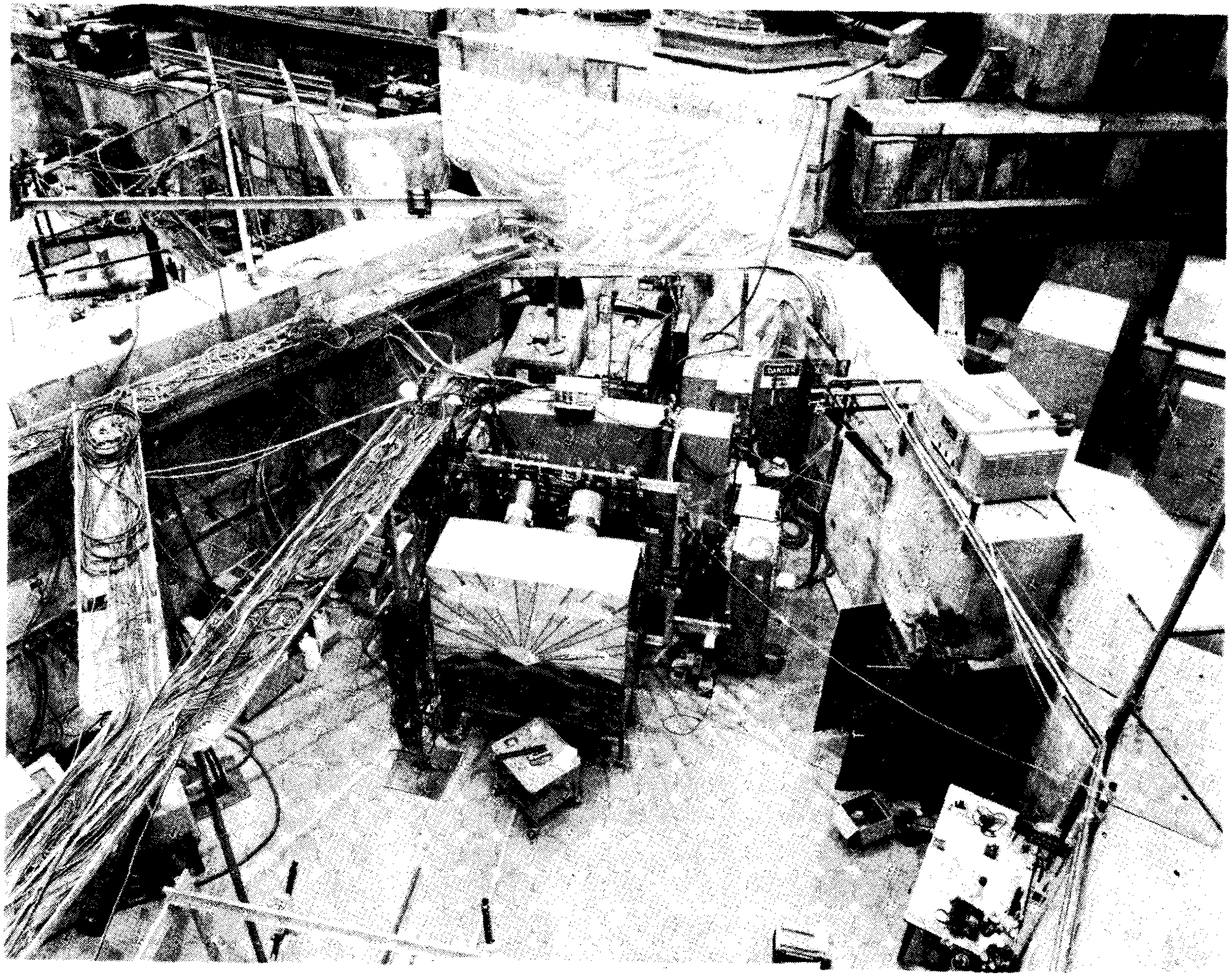

Fig. 33. Experimental arrangement for studying rare decay modes of π^0.

Experiment #31 — A Test of Muon Conservation
Yale, LASL, NRC – Canada, Saclay, SIN

$\mu^+ \rightarrow e^+ + \nu_e + \overline{\nu}_\mu$ additive or

$\mu^+ \rightarrow e^+ + \overline{\nu}_e + \nu_\mu$ multiplicative (both)

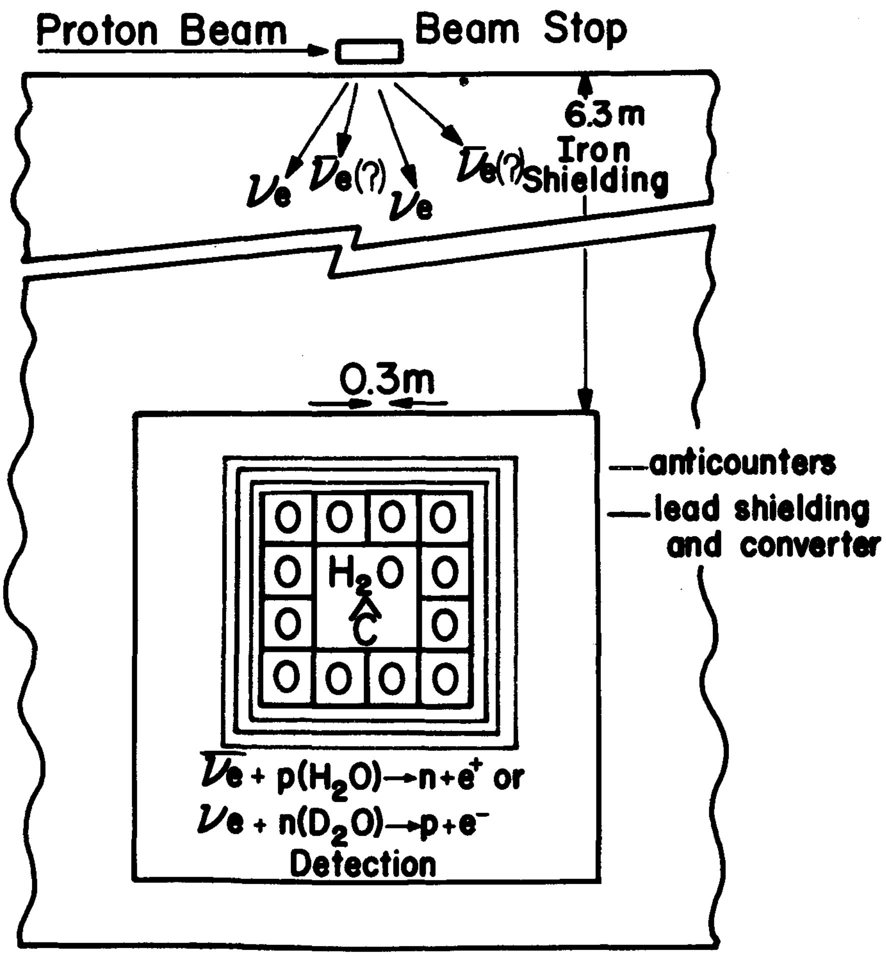

Schematic Top View

Fig. 34. Neutrino Interacting Detector.

$$\pi^- \; p \longrightarrow \pi^+ \; \pi^- \; n$$

C. W. Bjork, T. R. King, A. T. Oyer, G. A. Rebka, Jr.,
J. B. Walter - - Univ. of Wyoming
P.A.M. Gram, F. T. Shively - - LASL
C. Bordner - - Colorado College
R. Carawon - - North Carolina State Univ.
E. Lomon - - M. I. T.

Fig. 35. $\pi-\pi$ Interaction Investigators.

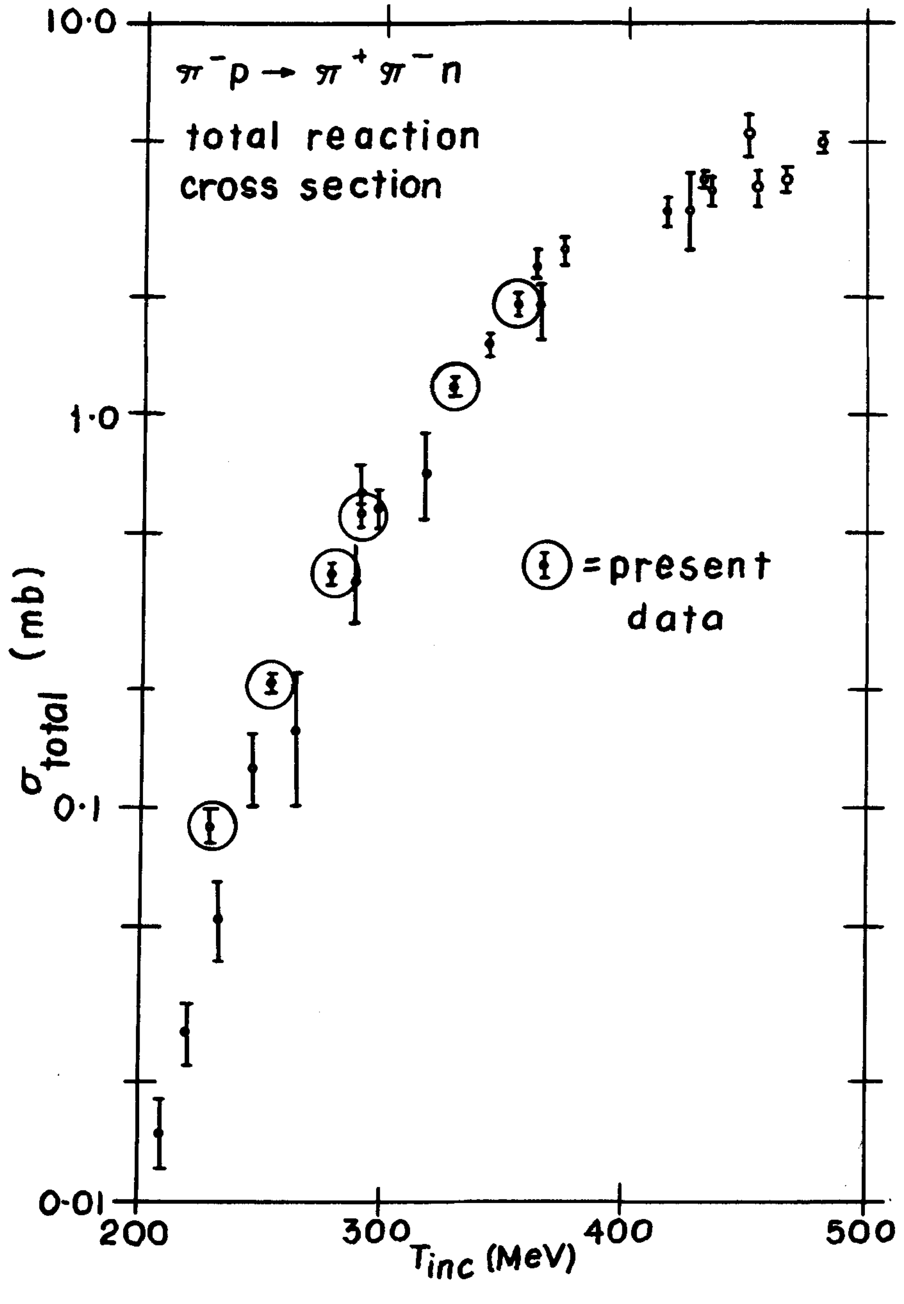

Fig. 36. Total Cross Section for
Two Pion Production.

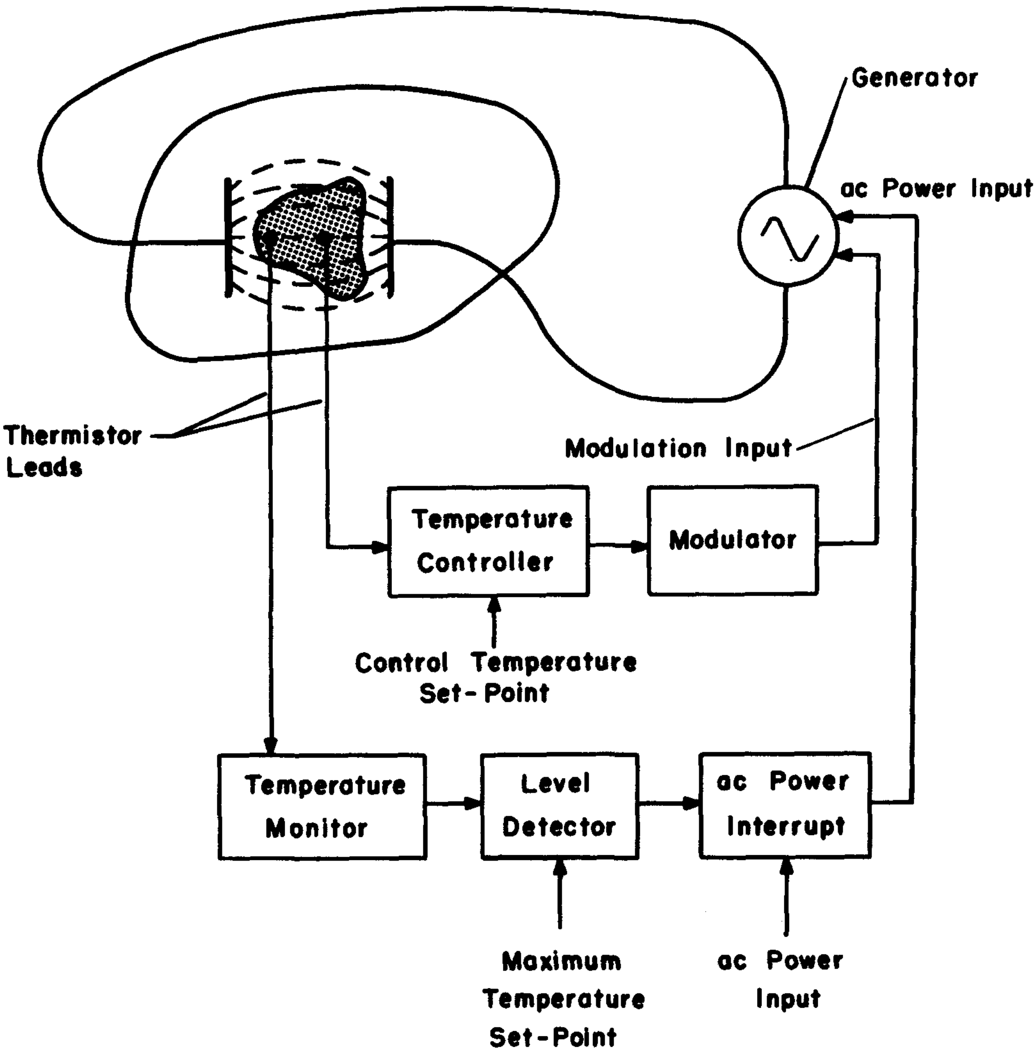

Fig. 37. Localized rf heating for tumor therapy.

#3 (HEREFORD)
July 1, 1976

10 WEEKS LATER
September 8, 1976

Fig. 38. Treatment of Cancer Eye with Localized rf Heating.

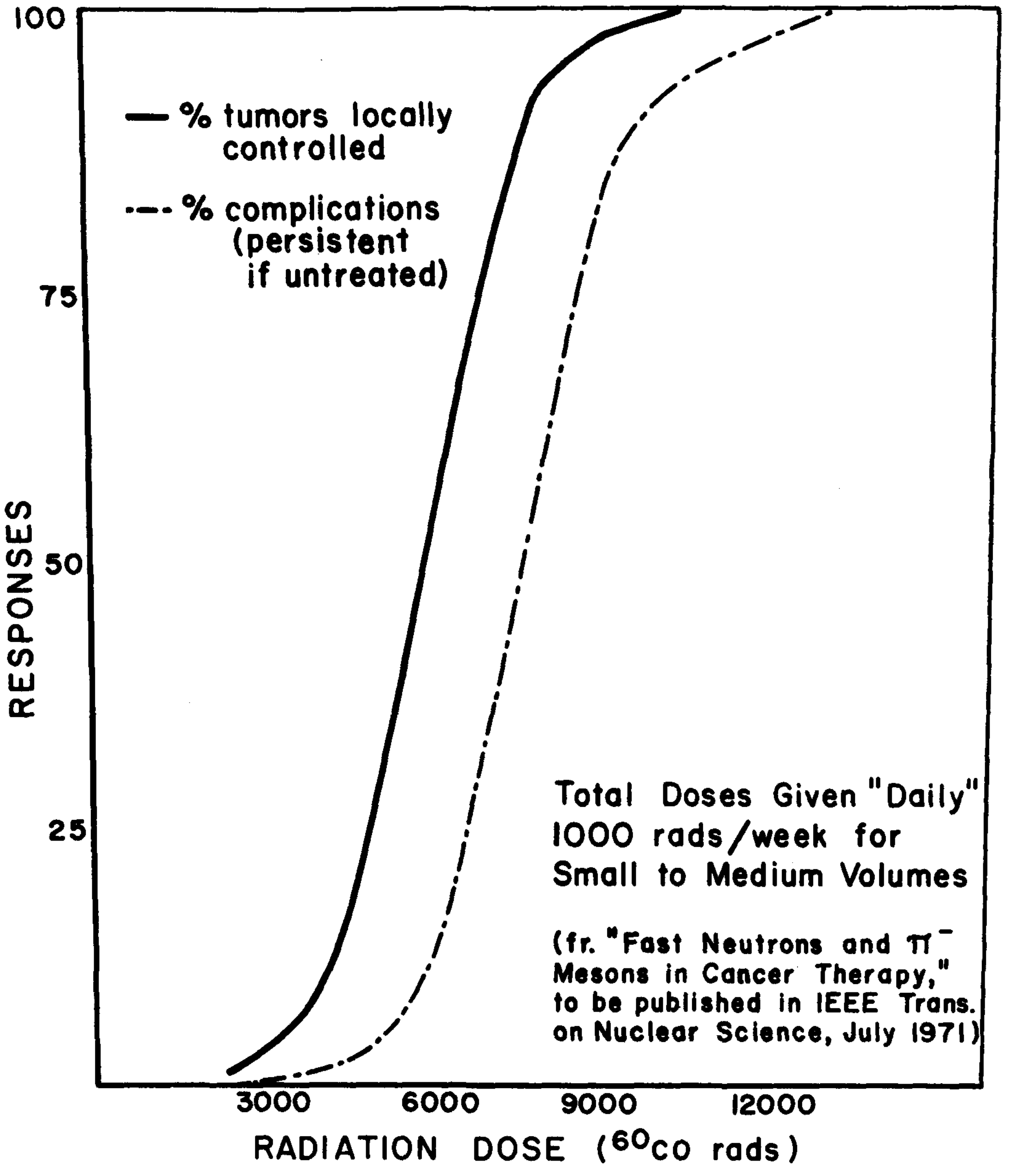

Fig. 39. Tissue Response as a Function of Dose in Normal and Diseased Tissue.

PLATE VI

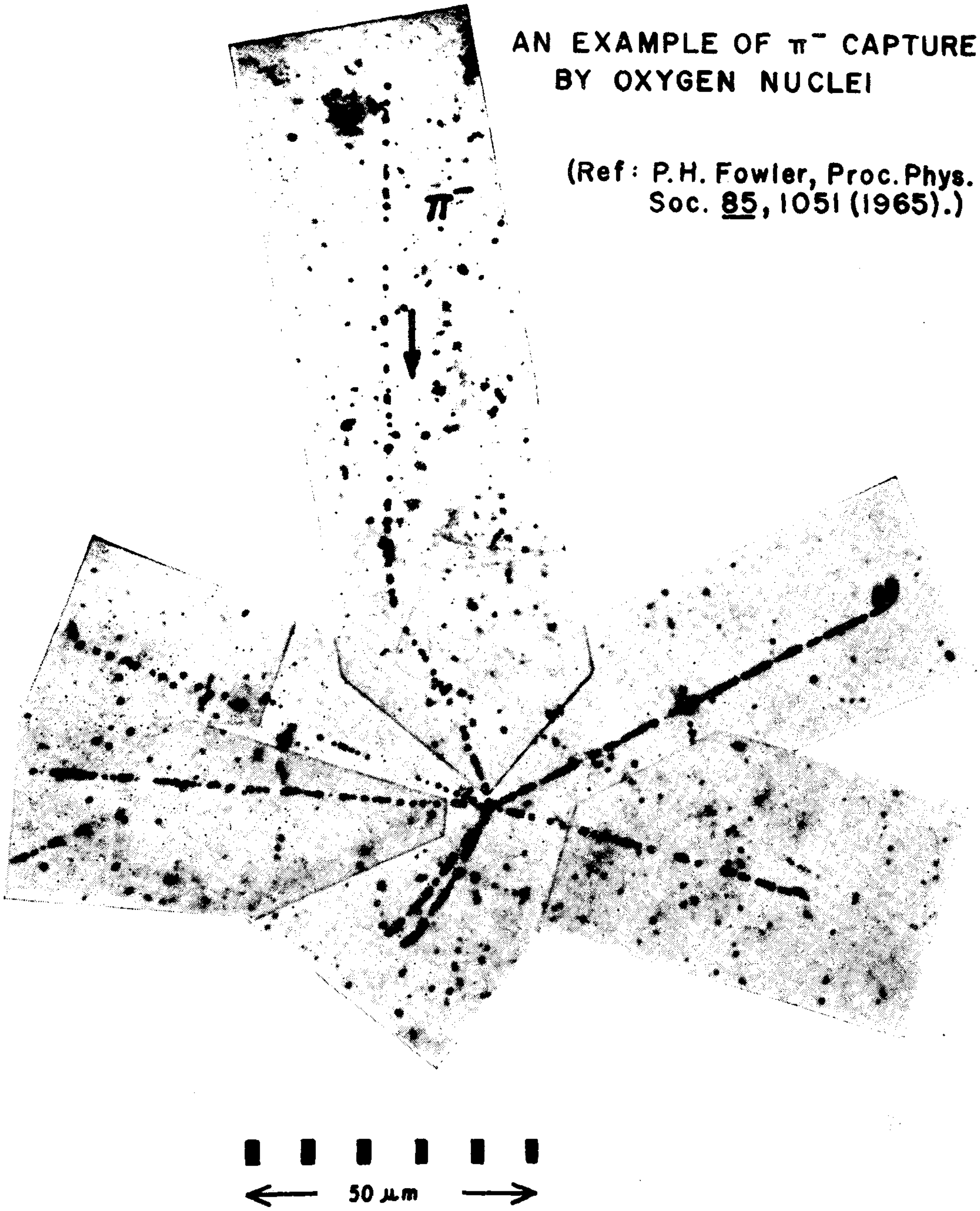

Fig. 40. Photomicrograph showing 'star' formation when negative pi meson comes to rest in matter.

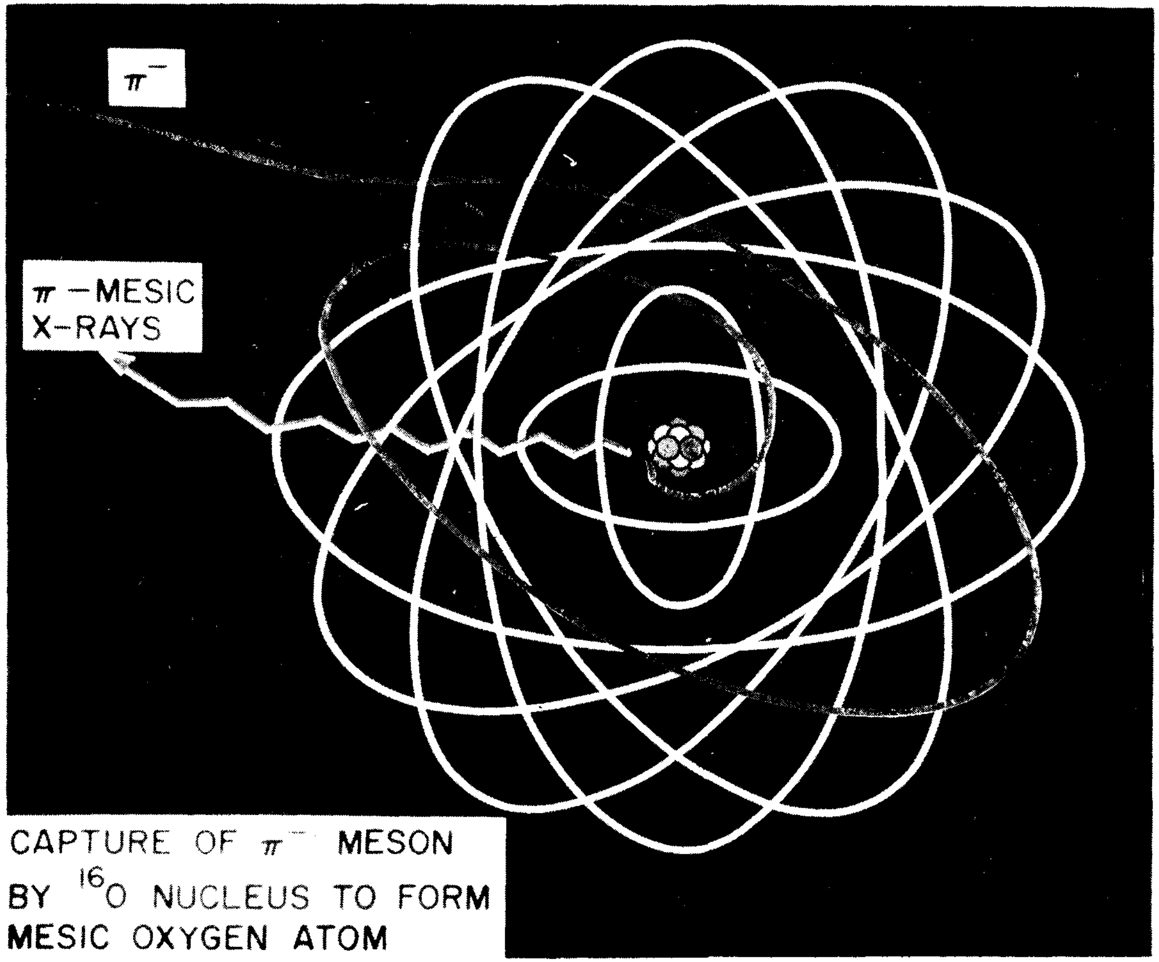

Fig. 41. Diagrammatic representation of a negative pi meson coming to rest in matter to form a mesic atom.

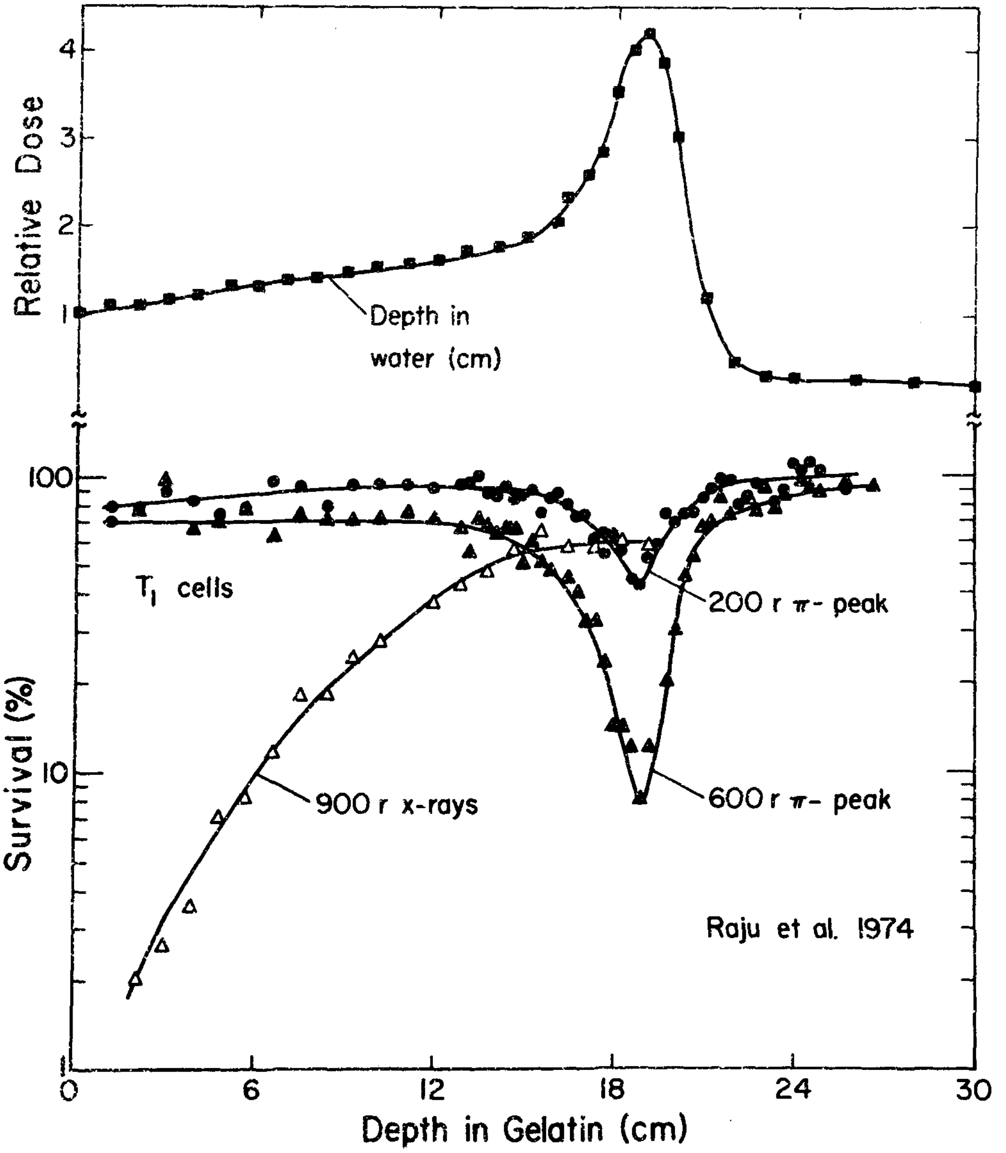

Fig. 42. Survival curves for T-1 human kidney cells when irradiated by x rays and negative pions.

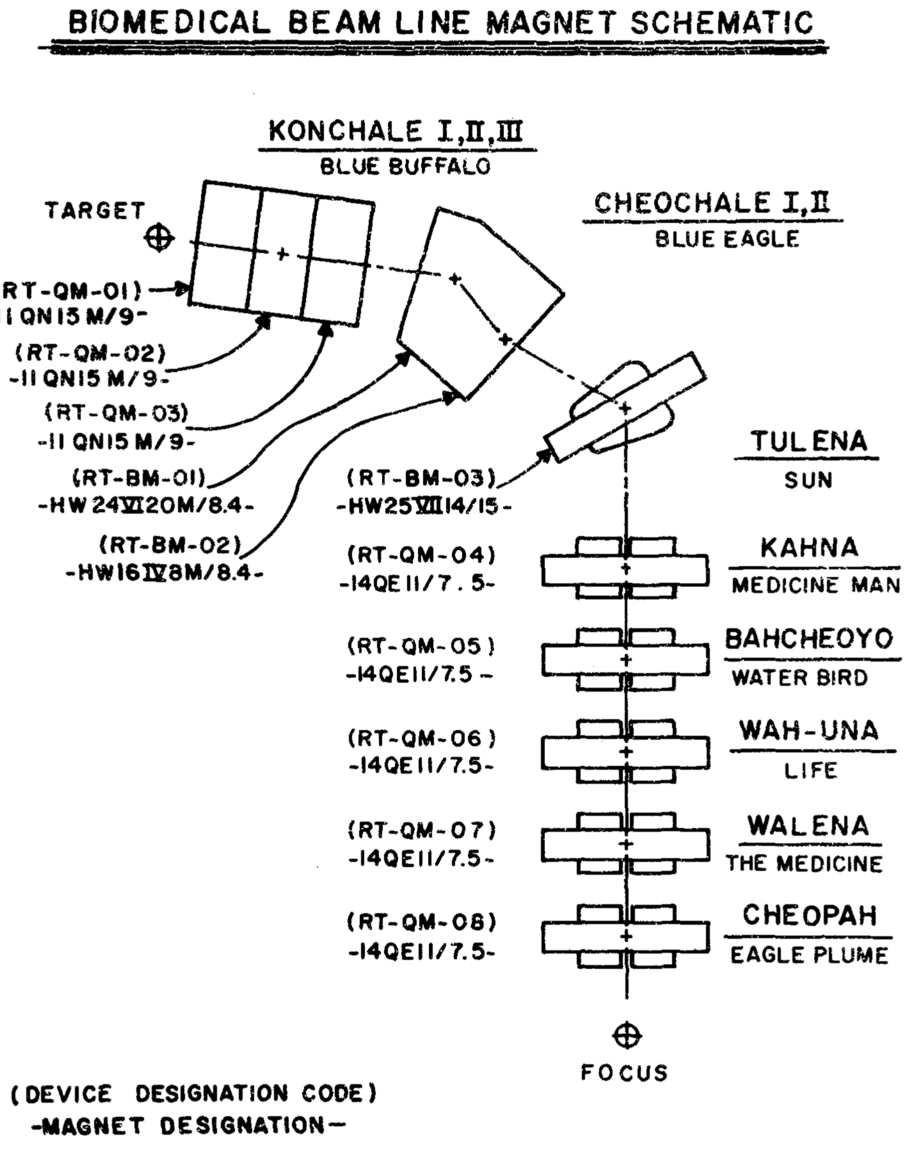

Fig. 43. Biomedical beam channel for pions up to 100-MeV energy.

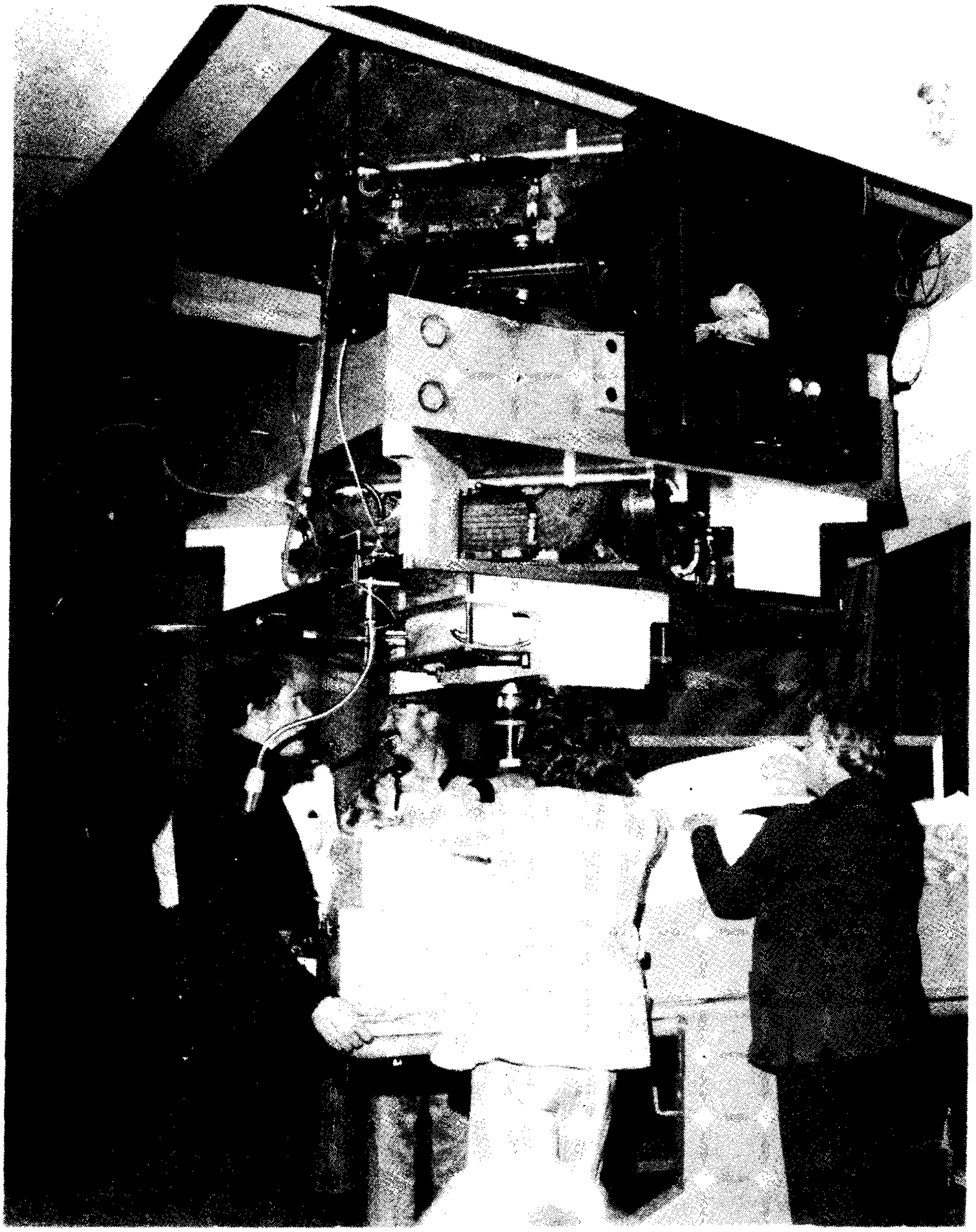

Fig. 44. First Patient Under Treatment with Pions.